TURBULENT FLAME SPEED MEASUREMENTS AND MODELING OF SYNGAS FUELS

Disclaimer

This report was prepared as an account of work sponsored by an agency of the United States Government. Neither the United States Government nor any agency thereof, nor any of their employees, makes any warranty, express or implied, or assumes any legal liability or responsibility for the accuracy, completeness, or usefulness of any information, apparatus, product, or process disclosed, or represents that its use would not infringe privately owned rights. Reference herein to any specific commercial product, process, or service by trade name, trademark, manufacturer, or otherwise does not necessarily constitute or imply its endorsement, recommendation, or favoring by the United States Government or any agency thereof. The views and opinions of authors expressed herein do not necessarily state or reflect those of the United States Government or any agency thereof.

Extended Abstract

This report summarizes the work done over the past three years involved with taking measurements of the turbulent flame speed, S_T, of syngas fuel blends at a variety of conditions. The objective of this work is to assess the extent to which varying fuel composition influences turbulent flame speeds – in other words, if two fuels have the same laminar flame speed, will their turbulent flame speeds also be the same or differ? Previous work has clearly shown that fuel does, in fact, exert powerful influences upon turbulent flame speeds. However, these data were obtained at relatively low turbulence intensities and velocities. As such, a key research question addressed was "Do fuel effects on turbulent flame speeds exert important influences at gas turbine realistic conditions?"

Measurements of the turbulent global consumption speed, $S_{T,GC}$, were obtained for atmospheric pressure H_2/CO flames for mean flow velocities and turbulence intensities of $4 < U_0 < 50$m/s and $1 < u'_{rms}/S_{L,0} < 100$ respectively, for H_2/CO blends ranging from 30-90% H_2 by volume. Two sets of experiments were conducted. Turbulent flame speeds were obtained with blends ranging from 30-90% H_2, with the mixture equivalence ratio, ϕ, adjusted at each fuel composition to have nominally the same unstretched laminar flame speed, $S_{L,0}$. The data clearly corroborate results from other studies that show significant sensitivity of $S_{T,GC}$ to fuel composition, in particular, that at a constant u'_{rms} and $S_{L,0}$, as the H_2 content increases $S_{T,GC}$ also increases. An important conclusion from this work was that fuel effects on $S_{T,GC}$ are not simply a low turbulence intensity phenomenon – they clearly persist over the entire range of turbulence intensities used in the measurements.

The constant $S_{L,0}$ studies were also extended to study length scale and preheat temperature. Specifically, measurements were obtained using a 12 mm burner diameter, for mean flow velocities ranging from 20-50 m/s to assess the influence of length scales on the flame speed measurements. It was found that the larger burner diameter flames exhibited larger average consumption speeds at a given fuel composition, turbulence intensity, and mean flow velocity. These differences are about 50% for 50 m/s and 60% for 30 m/s. Results of constant $S_{L,0}$ studies conducted at an elevated preheat temperature of 600 K and atmospheric pressure are also presented. Similarly, the turbulent flame speed is a function of fuel composition, with increasing

$S_{T,GC}$ as H_2 percentage increases. In the second set of experiments, the equivalence ratios were varied at fixed H_2 levels.

Taken together, these results clearly show that fuel composition exerts very significant impacts on turbulent flame speeds at conditions which approach those encountered in GT's (i.e., fuel effects are not a small lab scale, low turbulence intensity phenomenon only. This report also describes physics-based correlations of these data, using leading points concepts and detailed kinetic calculations of the stretch sensitivity of these mixtures. Finally, we develop an inequality for negative Markstein length flames that bounds the turbulent flame speed data and show that the data can be reasonably collapsed using the maximum stretched laminar flame speed, $S_{L,max}$, rather than $S_{L,0}$. The validity of this model has also been investigated through a G-equation model of the leading points.

Table of Contents

Table of Figures

1.   <u>Introduction</u>

There is significant interest in developing dry low NOx combustion technologies that can operate with synthetic gas (syngas) fuels derived from gasified coal or biomass [1]. Syngas fuels are typically composed primarily of H_2 and CO, and may also contain smaller amounts of CH_4, N_2, CO_2, H_2O, and other higher order hydrocarbons [2-3]. However, the specific composition depends upon the fuel source and processing technique, leading to substantial variability in composition - one of the largest barriers towards their usage in lean, premixed combustion systems.

A variety of operability, emissions, and structural life issues must be addressed in evaluating the impact of fuel composition on a gas turbine combustor; e.g., NOx and CO emissions, liner and fuel nozzle thermal loading, blow-off and flashback limits, and combustion instabilities. The turbulent flame speed is an important parameter through which the fuel composition exerts influences on many of these issues, such as thermal loading, blow-off limits, flashback limits, and combustion instability [4]. For example, the turbulent flame speed has a direct impact on the flame length and its spatial distribution in the combustor. This, in turn, affects the thermal loading distribution on the combustor liners, fuel nozzles and other hardware. Furthermore, the flames proclivity to flashback is directly a function of how rapidly the flame propagates into the reactants, which is dependent on the turbulent flame speed. In addition, the turbulent flame speed has a leading order influence on combustion instability limits through its influence upon the flame shape and length [5]. For example, measurements from Santavicca [6] have clearly shown how combustion instability boundaries are influenced by changes in flame location, due to changes in H_2 content of the fuel or mixture stoichiometry.

The unstretched laminar flame speed, $S_{L,0}$, is a thermo-physical property of a fuel-oxidizer mixture that describes the speed at which a laminar flame front propagates into a reactive mixture. For a given mixture, it is a function of pressure, temperature and flame stretch rate [7]. The turbulent flame speed, S_T, while having an analogous definition for the average propagation speed of a turbulent front, does not uniquely depend on the mixture's thermal and chemical properties. As with turbulence itself, S_T is a function of the flow within which the flame resides; i.e., it is a function of laminar flame speed, turbulence intensity, turbulence length

scales, etc. Correlations of turbulent flame speed of the form $\frac{S_T}{S_L} \# f\left(\frac{u'}{S_L}\right)$, where u' denotes the root mean square (RMS) turbulence fluctuation, have been obtained from numerous studies [8].

Numerous studies showing these fuel effects have been compiled in the review paper of Lipatnikov and Chomiak [9], and an updated discussion of stretch effects is provided by Driscoll [10]. These fuel effects are believed to be associated with stretch sensitivity of the reactive mixture, that is, in turn, a function of differences in the relative rates of mass and/or thermal diffusion of the deficient species [11]. Stretch sensitivity leads to variations in the local burning rate along the turbulent flame front. For example, the burning rate of the positively strained leading points of the turbulent flame is increased for mixtures with negative Markstein lengths, l_M [11]. Studies by Kido *et al.* [12] have shown that fuel/air mixtures with negative Markstein lengths (e.g., lean methane or hydrogen flames) have higher turbulent flame speeds than those that are relatively stretch insensitive, which, in turn, exceed those with positive Markstein lengths (e.g., lean propane-air flames). For syngas fuels, this effect is particularly important because of the large differences in diffusivity of the various fuel constituents (e.g., H_2 and CO, plus the diluents carbon dioxide (CO_2), nitrogen (N_2), and water (H_2O) with respect to each other and to air.

2.   Executive Summary

This report outlines measurements of the turbulent global consumption speed, $S_{T,GC}$, of atmospheric pressure H_2/CO flames. The measurements reported in this paper had two primary motivations. First, limited data are available for H_2/CO fuel mixtures; a few examples are from Daniele *et al.* [13] and Karpov and Severin [14]. Second, much of the turbulent flame speed data where strong stretch effects may be present have been obtained at turbulence intensities, $u'_{rms}/S_{L,0}$, often less than 20 [12, 15-21]. Obtaining such data at high turbulence intensities is of fundamental interest to explore the relative roles and interactions between turbulent stretching of the flame front and its stretch sensitivity, in particular whether stretch effects change with turbulence intensity. The above studies suggest that fuel effects persist at higher turbulence intensities, but further data are needed to validate this point. Measurements have been reported for mean flow velocities and turbulence intensities of $4 < U_0 < 50$m/s and $1 < u'_{rms}/S_{L,0}<100$ respectively, for H_2/CO blends ranging from 30-90% H_2 by volume. Two sets of experiments were conducted. Turbulent flame speeds were obtained with blends ranging from 30-90% H_2,

with the mixture equivalence ratio, ϕ, adjusted at each fuel composition to have nominally the same unstretched laminar flame speed, $S_{L,0}$. The data clearly corroborate results from other studies that show significant sensitivity of $S_{T,GC}$ to fuel composition, in particular, that at a constant u'_{rms} and $S_{L,0}$, as the H_2 content increases $S_{T,GC}$ also increases. An important conclusion from this work was that fuel effects on $S_{T,GC}$ are not simply a low turbulence intensity phenomenon – they clearly persist over the entire range of turbulence intensities used in the measurements.

The constant $S_{L,0}$ studies were also extended to study length scale and preheat temperature. Specifically, measurements were obtained using a 12 mm burner diameter, for mean flow velocities ranging from 20-50 m/s to assess the influence of length scales on the flame speed measurements. It was found that the larger burner diameter flames exhibited larger average consumption speeds at a given fuel composition, turbulence intensity, and mean flow velocity. These differences are about 50% for 50 m/s and 60% for 30 m/s. Results of constant $S_{L,0}$ studies conducted at an elevated preheat temperature of 600 K and atmospheric pressure are also presented. Similarly, the turbulent flame speed is a function of fuel composition, with increasing $S_{T,GC}$ as H_2 percentage increases. In the second set of experiments, the equivalence ratios were varied at fixed H_2 levels.

Taken together, these results clearly show that fuel composition exerts very significant impacts on turbulent flame speeds at conditions which approach those encountered in GT's (i.e., fuel effects are not a small lab scale, low turbulence intensity phenomenon only. In addition to the measurements, this report also describes physics-based correlations of these data, using leading points concepts [9, 22-23] and detailed kinetic calculations of the stretch sensitivity of these mixtures. The leading points concept provides a useful framework for incorporating modern understanding of stretch sensitivities of these flames [11] into data analysis. From this analysis we develop an inequality for negative Markstein length flames that bounds the turbulent flame speed data and show that the data can be reasonably collapsed using the maximum stretched laminar flame speed, $S_{L,max}$, rather than $S_{L,0}$. The validity of this model has also been investigated through a G-equation model of the leading points.

3.   Experimental Approach and Facility

This section describes the approach and experimental facility used to quantify the turbulent flame speed. As noted above, $S_{T,GC}$ is a property of not only the fuel-air mixture, but also the flow. As such, well characterized, highly reproducible burners whose results can be compared to other workers and data are critical to these measurements [24].

We start with some discussion of the measurement approach. This is an important issue because of the definition dependence of S_T. Extensive discussion of the merits and drawbacks of various approaches are contained in the literature. Some resolution has been achieved in two recent reviews [10, 25] and through the International Workshop on Premixed Flames [26], where it is noted that there are actually multiple useful definitions for S_T that are relevant for different combustion issues (e.g., flashback versus heat release per volume). Four definitions of S_T have been proposed: local displacement speed, $S_{T,LD}$, global displacement speed, $S_{T,GD}$, local consumption speed, $S_{T,LC}$, and global consumption speed, $S_{T,GC}$ [12, 17, 18]

The local consumption and displacement speeds attempt to quantify the local propagation rate and mass burning rate of the turbulent front, respectively. There are various problems associated with defining these quantities locally, however. For example, the definition of $S_{T,LC}$ is:

$$S_{T,LC} = \Sigma \int_{-\infty}^{\infty} \eta \tag{1}$$

where $S_{L,0}$, I_0 and Σ are the unstrained laminar flame speed, stretch factor and the flamelet surface area per unit volume respectively. Clearly, this integral is a function of the integration path, η, through the turbulent flame brush. Several authors suggest that it be performed in a direction normal to the flame brush [10], which is itself usually a function of reaction progress variable.

Difficulties associated with defining a local value of S_T can be circumvented to some extent by defining global burning rates (assuming, of course, that all the reactant mass flow pass through the flame brush [10]), at the cost of averaging over potentially substantial variations in local burning rates for cases where the flame brush is spatially evolving. However, global turbulent flame speeds are also definition dependent. For example, $S_{T,GC}$ is defined as:

$$S_{TGC} = \frac{\dot{m}_R}{\rho_R \overline{A}_{<c>}}$$ (2)

where $\dot{m}_R$, ρ_R and $\overline{A}_{<c>}$ denote reactant mass flow rate, reactant density and mean flame area corresponding to some prescribed $<c>$ contour. Thus, the value of $S_{T,GC}$ is itself a function of which progress variable surface is used to define the mean flame front area.

This study focuses upon measurements of $S_{T,GC}$ using a turbulent Bunsen flame, an $S_{T,GC}$ measurement approach recommended by Gouldin and Cheng [26]. This configuration was used because of the wide variety of available data in similar geometries for benchmarking and comparisons.

A schematic of the system is shown in Figure 1. The burner is a smoothly contoured nozzle with high contraction ratio to inhibit boundary layer growth and to achieve a top hat exit velocity profile. Measurements were taken using burners with 12 and 20 mm exit diameters. An annular sintered plate is placed around the burner outlet to hold a premixed, methane-air pilot flame, needed to stabilize the main flame at the higher flow velocities used in this study. The total mass flow rate of the pilot does not exceed 5% of the main flow rate to ensure minimal impact of the pilot on the main flame. This was checked by taking measurements with various pilot flow rates.

Mass flow rates of the fuel and air for both the main and pilot flames are metered using mass flow controllers that have accuracies of ±1.5% of the full scale. As a result, equivalence ratios quoted here have uncertainties ranging from 3% to 5%, depending on the full-range scale of the mass flow controllers used.

The fuel/air mixture is premixed 2 m ahead of the burner. Upon entering the main burner assembly, the flow passes through a layer of ball bearings to minimize "jetting" effects from the smaller diameter reactant feed lines.
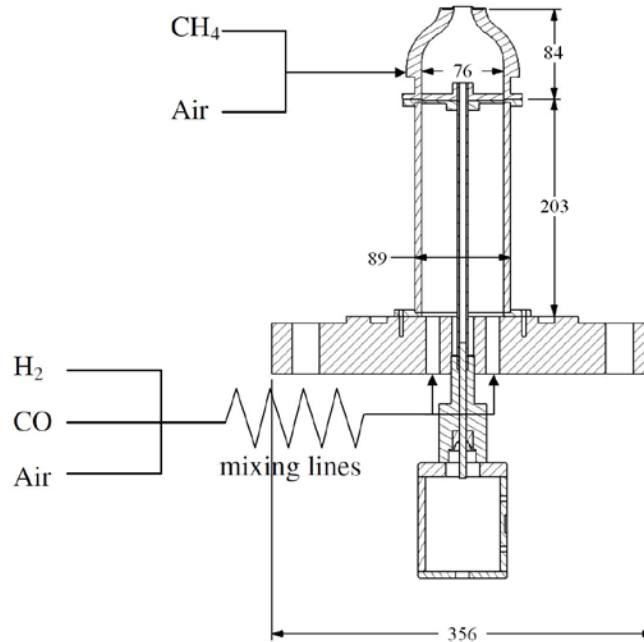
Figure 1: Schematic of the experimental facility. Dimensions in mm.

The turbulence intensity is varied independently of the mean flow velocity using a remotely controlled turbulence generator. This turbulence generator assembly consists of milled slots in a thin plate that cause flow separation and vorticity generation as the flow passes through them. These vortical structures impinge on the inclined wall of the converging section of the nozzle, breaking them down into finer turbulent eddies [27-29].

As shown in Figure 1, the turbulence generating plates are secured 84 mm upstream of the burner exit. Prior implementations of these turbulence generators used fixed plates [27-29] – different blockage ratio plates were manufactured to vary turbulence intensity. In this study, substantial effort was devoted to developing a system that is continuously variable, in order to sweep out a range of turbulence intensities at a fixed mean flow velocity. This capability is also needed to facilitate the high-pressure measurements that are planned for the next phase of experiments. This system consists of a 3 mm thick bottom plate that is secured to the plenum and a 6 mm thick top plate attached to a central shaft that is connected to a stepper motor. This configuration allows for variable degrees of blockage as shown in Figure 2.
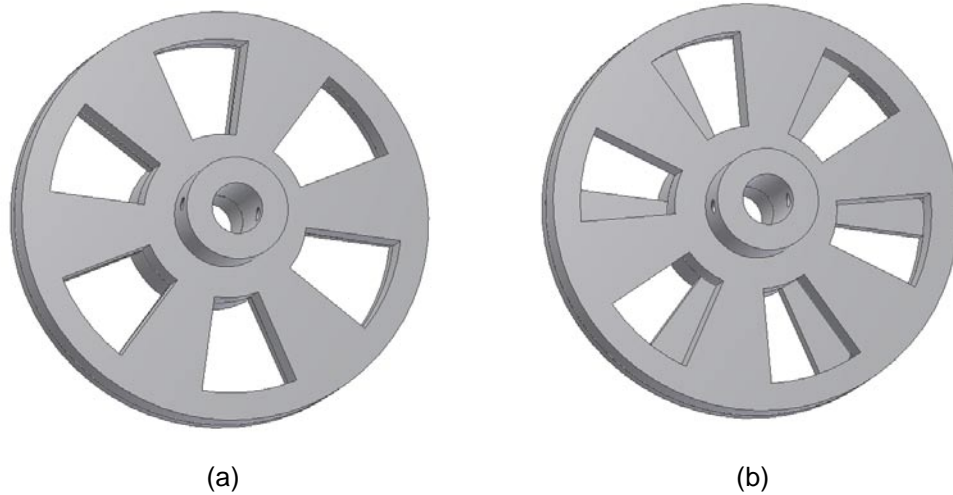
Figure 2: Schematic of the turbulence generating plates: (a) fully open and (b) partially closed.

The plate's angular position is measured with an optical encoder to an accuracy of ±0.1°. The stepper motor is connected to the central shaft via a worm gear, minimizing backlash. Maximum and minimum blockage possible with this setup is 97% and 69%, corresponding to an angular opening of 1.5 degrees and 30 degrees, respectively. Turbulence intensity increases monotonically with increasing blockage ratio.

At very high blockage ratios, the mixture passes through the slots at an angle, leading to some swirl in the flow. This effect was reduced somewhat by the addition of straighteners as shown in Figure 3, but it still imposes a maximum blockage ratio over which data are obtained. We utilized the criterion that the maximum blockage ratio remains less than 93% for all flame speed data presented in this paper, based upon the flow field characterization described in the next section.
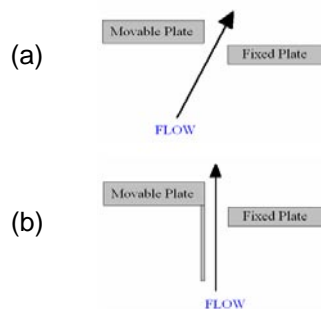
Figure 3: Flow characteristics (a) without and (b) with flow straighteners.

3.1.   Flow Field Characterization

The flow field was characterized using a TSI 3-component Laser Doppler Velocimetry (LDV) system. The flow was seeded using 5 µm alumina (Al_2O_3) particles. Data were obtained at mean flow velocities from $U_0 = 4 - 50$ m/s, which correspond to $Re_D = U_0D/\nu = 5,100 - 64,000$. The turbulence intensities quoted below, u'_{rms}, are based upon the total turbulence intensity using all three velocity components; i.e., $u''''_{rms} = \sqrt{\overline{u^2} + \overline{v^2} + \overline{w^2}}$. As such, some care should be taken when comparing with other data in the literature, such as when measurements are obtained with hot wire anemometers that capture two velocity components.

Figure 4 through Figure 6 plot representative profiles of the mean and fluctuating axial, radial and azimuthal velocities as a function of the radial distance from the center of the 20mm diameter burner at 50m/s at three different blockage ratios.
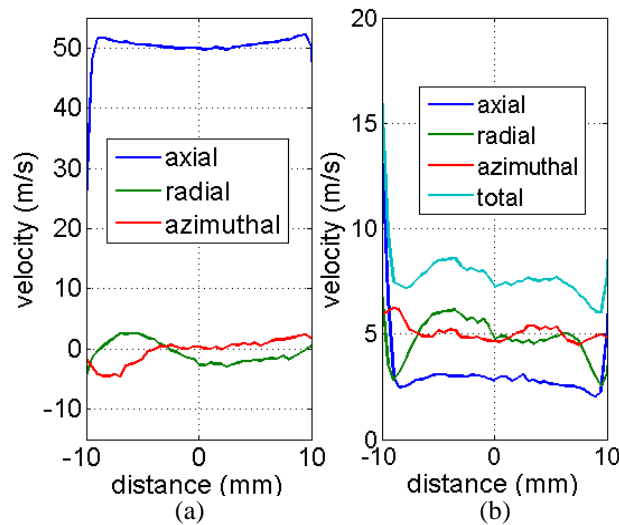
Figure 4: Plots of (a) mean axial, radial and azimuthal velocities and (b) fluctuating axial, radial, and azimuthal and total fluctuating velocities as a function of radial distance from center of the burner for $U_0 =$ 50m/s at a blockage ratio of 69%.
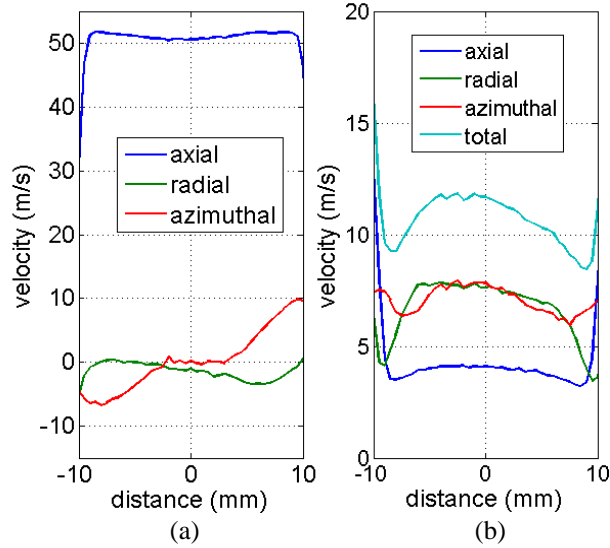
Figure 5: Plots of (a) mean axial, radial and azimuthal velocities and (b) fluctuating axial, radial, and azimuthal and total fluctuating velocities as a function of radial distance from center of the burner for $U_0 =$ 50m/s at a blockage ratio of 81%.
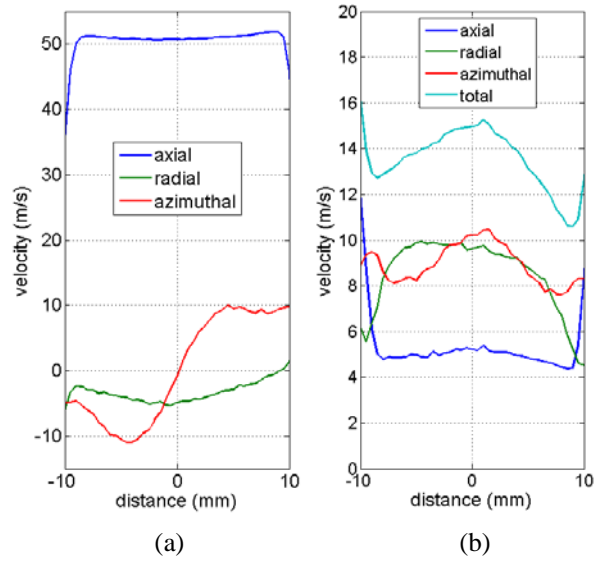
Figure 6: Plots of (a) mean axial, radial and azimuthal velocities and (b) fluctuating axial, radial, and azimuthal and total fluctuating velocities as a function of radial distance from center of the burner for $U_0 =$ 50m/s at a blockage ratio of 93%.

The data show a well-defined top-hat mean axial velocity, along with low radial velocity. The azimuthal velocity increases with increasing blockage ratio, as discussed earlier. It should be noted that the time averaged mean and fluctuating velocities are flat, except in the boundary layer, and that as the blockage ratio is increased from 69% in Figure 4 to 93% in Figure 6, the turbulence intensity increases.

Figure 7 summarizes the performance of the turbulence generator, by plotting the centerline turbulence intensity, u'_{rms}/U_0 as a function of the blockage ratio. It shows that the

turbulence intensity monotonically increases with blockage ratio. The 12 mm burner has a lower turbulence intensity than the 20 mm burner at the same blockage ratio. This occurs because the flow velocity through the blockage plate gaps is lower for the smaller burner (note that the nozzle exit velocity is what is fixed).
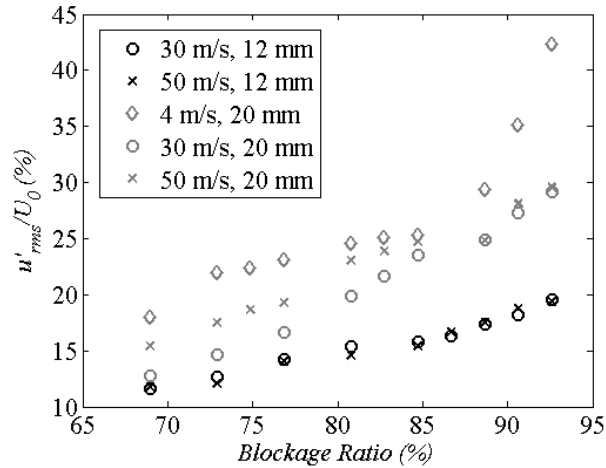
Figure 7: Dependence of burner centerline total turbulence intensity (i.e. summed over all 3 fluctuating velocity components) upon blockage ratio.

An important question for configurations such as used here, where the turbulence intensity varies radially and axially, and where there is strong shear generated turbulence, is the appropriate turbulence intensity that should be used to characterize u'_{rms}. While we do not weigh in on this question here, we do note that the centerline turbulence intensity scales well with that at other locations. To illustrate, Figure 8 presents a comparison between the shear (or, more precisely, u'_{rms} at $r = 10$ mm) and centerline turbulence intensities. Note the one-to-one correspondence between the two, with $u'_{rms}(r = 10 \text{ mm}) = 0.87 u'_{rms} (r = 0 \text{ mm}) + 6.9 U_0$.
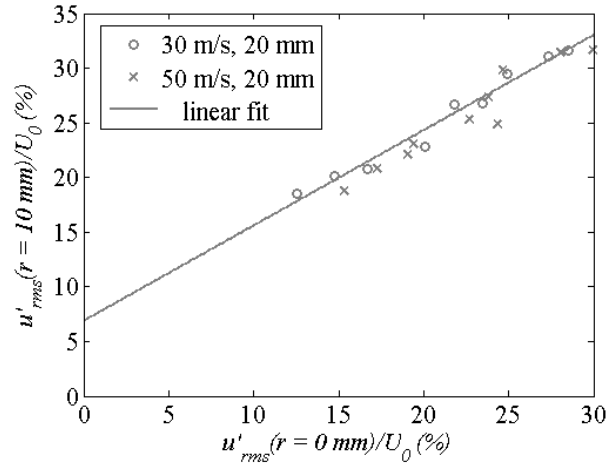
Figure 8: Comparison of turbulence intensity in shear layer and burner centerline.

Limited particle image velocimetry (PIV) were also conducted to map the entire flow field and determine the axial dependence of the turbulence intensity. Figure 9 shows the mean and RMS velocity fields normalized by the mean centerline velocity at the burner exit. Note that the centerline turbulence intensity remains relatively constant, and actually grows slightly for at least the first 50 mm downstream, typical of jet turbulence [30]. This is important since it implies that the turbulence intensity at the flame front is approximately the same as the intensity at the burner exit.
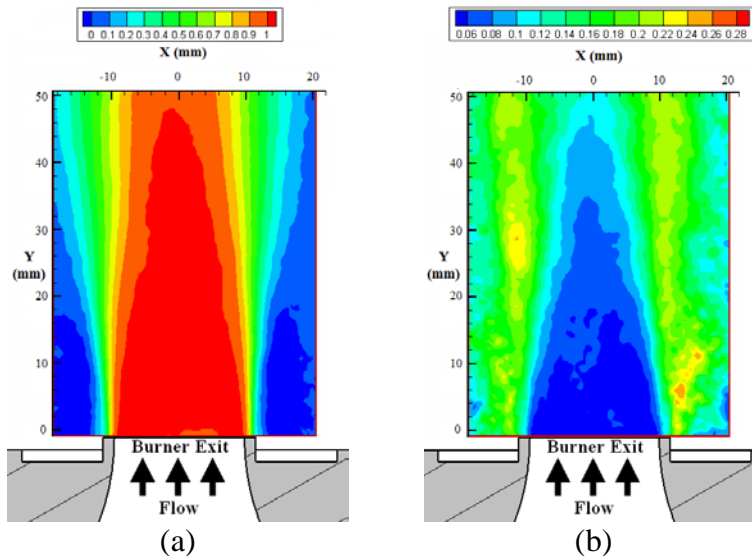
Figure 9: PIV velocity data for the 20mm burner at a blockage ratio of 80% for U_0 = 4m/s a) mean velocity normalized by the centerline mean velocity at the burner exit b) RMS velocity normalized by the centerline mean velocity at the burner exit.

Figure 10 presents typical 1-D turbulent power spectra at the burner centerline for several blockage ratios at U_0 = 4 m/s for the 20mm burner diameter. The data were obtained from autocorrelations of the LDV time series, described later. The spectra show a smooth roll-off with increasing frequency, and that there are no discrete peaks, as desired. The graph shows that the power spectrum values increases with blockage ratio.
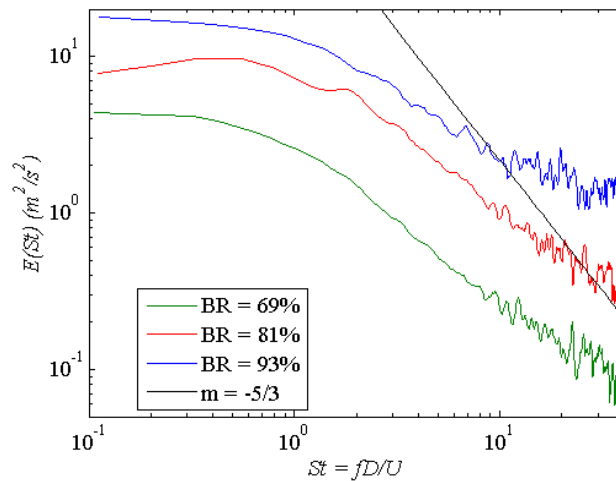
Figure 10: 1-D turbulent power spectra as a function of Strouhal number St for U_0 = 4m/s at 3 different blockage ratios for the 20mm burner diameter

Integral time scales, t_{int}, were determined from autocorrelations of the centerline velocity data. The autocorrelation function was determined from Equation (3) using the slotting technique of Mayo [31] with the local normalization improvement described by Tummers [32]:

$$\rho(k\Delta\tau) = \frac{\sum_{i}^{N}\sum_{j=i+1}^{N} u_i u_j b_k(\Delta\tau)}{\sqrt{\sum_{i}^{N}\sum_{j=i+1}^{N} u_i^2 b_k(\Delta\tau)} \quad (\quad)} \tag{3}$$

for: $0,1,...M$

where $b_k\left(\Delta\tau\right) = \left(\quad-\quad\right)_{ij}$, $M = \dfrac{\tau_{max}}{\Delta\tau}$, τ_{max} is the maximum lag time, and $\Delta\tau$ is the slot width. The integral time scale was defined using the relationship:

$$t_{int} = \int_{0}^{\infty} \rho(\tau) \, d\tau \tag{4}$$

Because of the high uncertainties associated with the autocorrelation at large time lags (because of its low value), an exponential expression of the form $\rho(\tau) = a e^{-b\tau}$ ( ) was fit to the autocorrelation function and used to evaluate this integral, so that t_{int} is given by Equation (5). A typical result is shown in Figure 11.

$$ t_{int} = \frac{a}{b} + \frac{1-}{c} \tag{5} $$
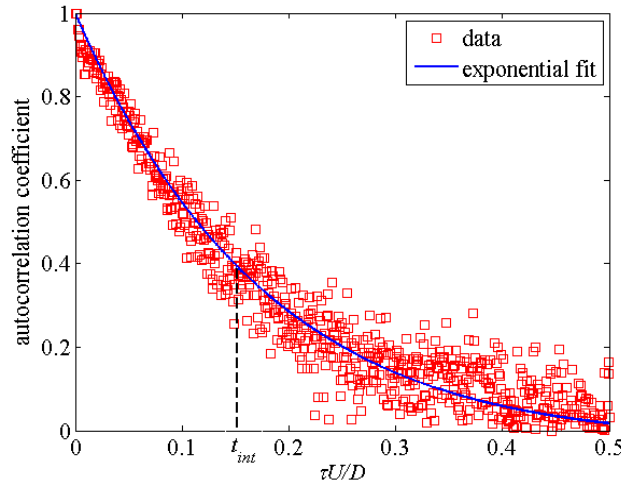
Figure 11: Autocorrelation coefficient plotted against normalized lag time for U_0 = 4m/s, blockage ratio = 93%, 20mm burner diameter

These integral time scales were converted to integral length scales, l_{int}, using the relation $l_{int} = t_{int}U_0$, as per Taylors' hypothesis. Figure 12 summarizes the calculated l_{int}/D values at mean flow velocities of 4, 30, and 50 m/s at various blockage ratios. The data indicate that l_{int}/D is nearly constant at 30 and 50 m/s, and changes slightly with blockage ratio. These data show that turbulence length scales are not varying with blockage gap width and therefore, that the associated variations in turbulence intensity are at essentially constant integral length scale. The t_{int} values in the 4 m/s case are substantially higher in value and do indicate a somewhat higher sensitivity to blockage ratio. It is assumed that this reflects a different characteristic of the turbulence generator system at the much lower Reynolds numbers these data were obtained.
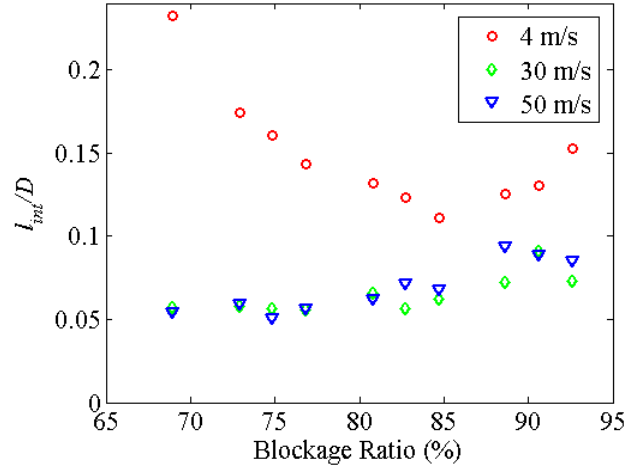
Figure 12: Comparison of integral length scale (normalized by burner diameter) vs. blockage ratio at 4, 30, and 50m/s.

3.2. Image Analysis

Global consumption speeds were calculated using Eq. (2), whose key measurement input is progress variable surface area, $\overline{A}_{\langle c \rangle}$. This section describes the approach used to determine this surface area.

Digital images of the flame emission are captured with a 16-bit intensified charge-coupled device (ICCD) camera with a resolution of 512 x 512 pixels and a 105 mm, f/4.5, UV camera lens. The camera system is sensitive in the visible and ultraviolet regions (~220-650 nm) and, hence, is capable of capturing both OH* and CO_2* chemiluminescence. This is important for high hydrogen content fuels since the OH* chemiluminescence associated with hydrogen flames emits in the UV range.

Line of sight images of the flame were obtained over 5 seconds and time-averaged; see Figure 13(a). These averaged images are nearly symmetric about the centerline. The left and right halves were then averaged and filtered with a 2-D median filter with a kernel size that is less than 2% of the burner diameter. Note that other potential Bunsen flame $S_{T,GC}$ measurement approaches include Mie scattering [33-34] or OH-PLIF [35] measurements for flame characterization. The resulting progress variable contours (described below) are equivalent for the two methods, assuming that the OH-PLIF or Mie interface surface is equivalent to the chemiluminescence flamelet surface [36-37]. This line-of-sight approach was used here, however, because the OH-PLIF or Mie scattering technique does not capture flame surface

density in the out-of-plane direction and, as such, significantly underestimates it. The spatial distribution of heat release is fully captured by a line of sight measurement.

To estimate the time-averaged flame brush location from the line-of-sight images, a three-point Abel deconvolution scheme [38] was used; see Figure 13(b). The axial distribution of the centerline intensity is then fit to a Gaussian curve, from which the location of the maximum intensity is identified. This point is associated with the most probable location of the flame, and defined as the $\langle c \rangle = 0.5$ progress variable contour. The estimated uncertainty in identifying this point is 1-2%. The other progress variables were then defined by the following relation:

$$\langle c \rangle = \begin{cases} \dfrac{I}{I_{max}} & \langle c \rangle \le 0.5 \\[4mm] 1 - \dfrac{I}{I_{max}} & \langle c \rangle > 0.5 \end{cases} \tag{6}$$

Straight lines are then drawn from this point to the two flame anchoring points and rotated about the line of symmetry to generate a cone. The $\langle c \rangle = 0.5$ surface is drawn in Figure 13(b). This method was used to aid in comparing the results of this study with other data in the literature where a similar method was used to determine the flame area (e.g., the "angle method") [33-34, 39].
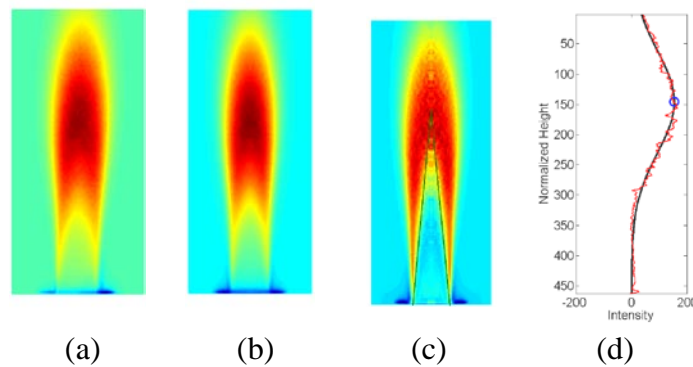
Figure 13: Time averaged, line of sight flame images showing (a) background subtracted image, (b) axisymmetric image and (c) Abel inverted image with <c> = 0.5 contour shown (d) plot of intensity as a function of image height used to determine contours. The red and black lines represent the raw data and fitted data respectively.

From Figure 13 it is clear that the surface used to determine $\bar{A}$ does not coincide with the actual flame $\langle c \rangle = 0.5$ surface except at the centerline. However, this method was used to aid in comparing the results of this study with other data in the literature where a similar method was used to determine the flame area (e.g., the "angle method") [24, 40]. In future publications we

will report the sensitivity of the results to this surface location; however, we believe that all trends observed will remain unaltered.

As noted earlier, $S_{T,GC}$ is a function of the progress variable, $<c>$, used to define $\bar{A}$. Figure 14 plots the dependence of $S_{T,GC}$ upon the progress variable contour, $<c>$, at several H_2/CO ratios. As expected, $S_{T,GC}$ decreases with increasing $<c>$ value. This graph also shows that the different H_2/CO ratio flames have similar dependence upon $<c>$ contour. It also shows, however, that the highest H_2 mixture (90/10 mixture), does have the least sensitivity to $<c>$, illustrating that the flame brush thickness is decreasing with increased H_2 content.
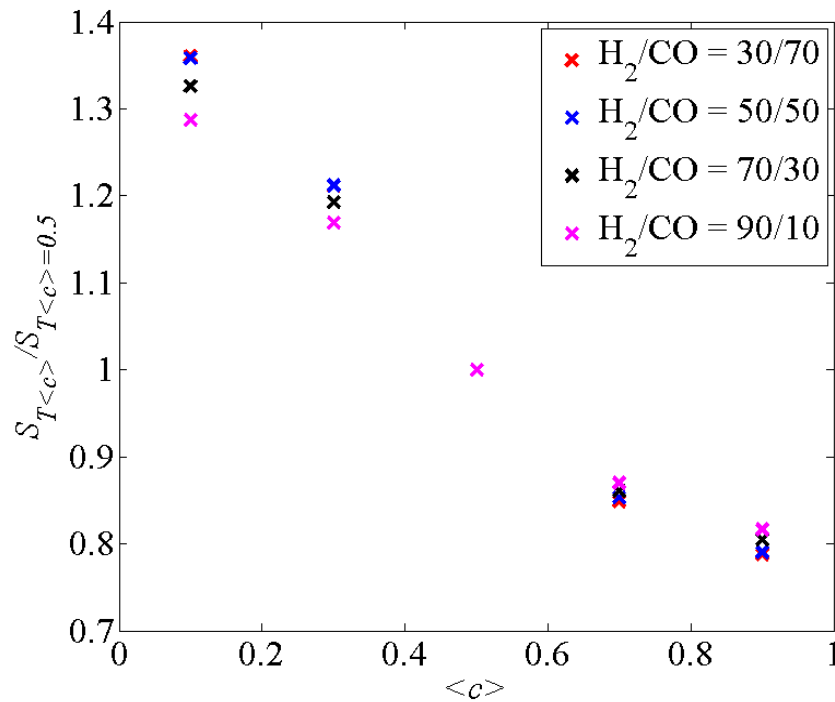
Figure 14: Dependence of $S_{T,GC}$ value upon using different progress variable normalized by $S_{T,GC<c>=0.5}$ as a function of the progress variable for different H_2/CO ratios at 50m/s and $u'/S_{L,0}$ = 22.5, and $S_{L,0}$ = 0.34m/s.

The overall uncertainty in the estimated $S_{T,GC}$ (as defined in this report) value is then estimated to be 3%.

4.   Results and Discussion

Two basic sets of tests were performed. Measurements of $S_{T,GC}$ were obtained as a function of $u'/S_{L,0}$ for 12 and 20 mm burner diameters at mean flow velocities from 4-50 m/s and volumetric H_2/CO ratios from 30/70 – 90/10, keeping $S_{L,0}$ and reactant temperature fixed at 34 cm/s and 300 K respectively. $S_{L,0}$ was kept nominally constant by adjusting the stoichiometry at each H_2/CO ratio. Additionally, a CH_4/air data set was obtained at the same $S_{L,0}$ ($\phi = 0.9$). $S_{L,0}$ estimates were determined using the CHEMKIN software with the Davis H_2/CO mechanism for H_2/CO mixtures [41] and GRI 3.0 for CH_4/air [42]. Symbol type and color scheme for this data set are summarized in Table 1 and Table 2.

The complete flame speed data set has been summarized in Figure 16 below.

Table 1: Legend used for the constant $S_{L,0}$ data set for the 20mm burner at 1atm

Table 2: Legend used for the constant $S_{L,0}$ data set for the 12mm burner at 1atm

Global consumption speed measurements were also obtained at atmospheric pressure and elevated preheat temperature of 600K for mean flow velocities ranging from 20m/s to 50m/s. The constant $S_{L,0}$ studies were conducted at $S_{L,0} = 2$m/s so that the equivalence ratios were not very lean.

Table 3: Legend used for the constant $S_{L,0}$ data set at $T_u = 600K$ for the 20mm burner at 1atm

		Velocity (m/s)				
		20		30		50
P (atm)		1	5	1	5	1
H₂ (%)	30	▽	◖	+		△
	50		◖	+		
	70		◖	+	×	△
	90	▽	◖	+	×	△

The second set of tests was performed by sweeping the equivalence ratio at constant H₂/CO ratio values of 30/70 and 60/40 with the 20 mm burner. The symbol type and color scheme used for this data set are summarized in Table 4.

Table 4: Legend for constant H_2 content equivalence ratio sweeps data for the 20mm burner

		Velocity (m/s)			
H₂	Φ	4	10	30	50
30	0.59	★	★	★	★
	0.7	✳	✳	✳	✳
	0.8	▽	▽	▽	▽
60	0.4	▷	▷	▷	▷
	0.6	✖	✖	✖	✖
	0.8	◻	◻	◻	◻
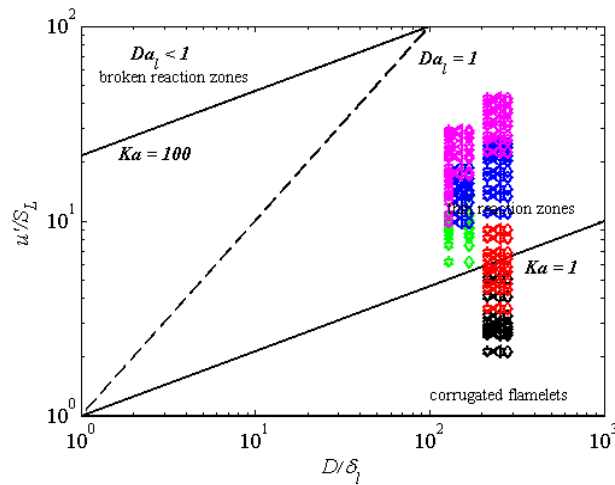
Figure 15: Borghi diagram showing location of data.
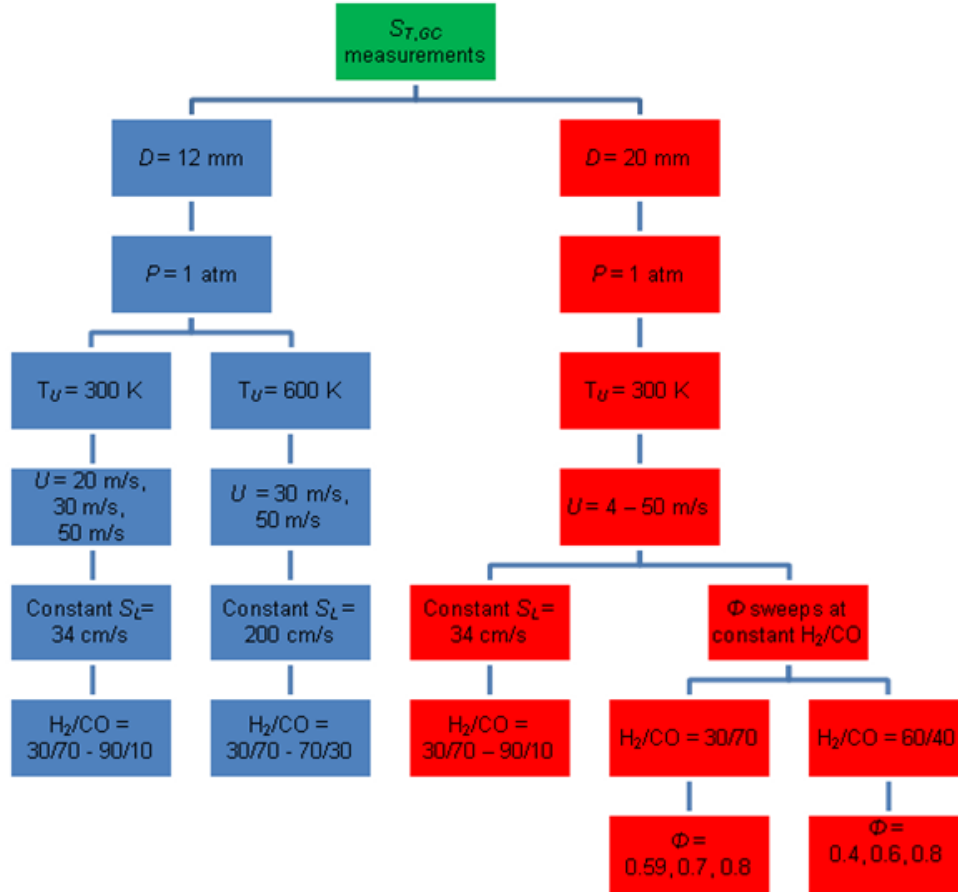
Figure 16: Flame speed measurements data set

Flame speed stretch sensitivities were also calculated using an opposed flow calculation of two premixed flames with a nozzle separation distance of 20 mm, using the OPPDIF module in CHEMKIN. From these calculations various properties of the strained values were extracted. The S_L value reported here is defined as the minimum velocity just ahead of the reaction zone, as suggested by Wu and Law [43]. The Markstein length, l_M, was determined from the slope of the linear fit in the low strain regime of the κ vs. S_L curve. Extinction strain rates, κ_{ext}, were calculated using an arc length continuation method [44]. An example set of calculations for the constant $S_{L,0}$ mixtures are show in Figure 17, showing that the mixtures converge to the same $S_{L,0}$ at $\kappa = 0$. However, they clearly have different stretch sensitivities as quantified by the Markstein length and extinction strain rates. These stretch sensitivities are used later in the flame speed correlation section to facilitate analysis of these data.
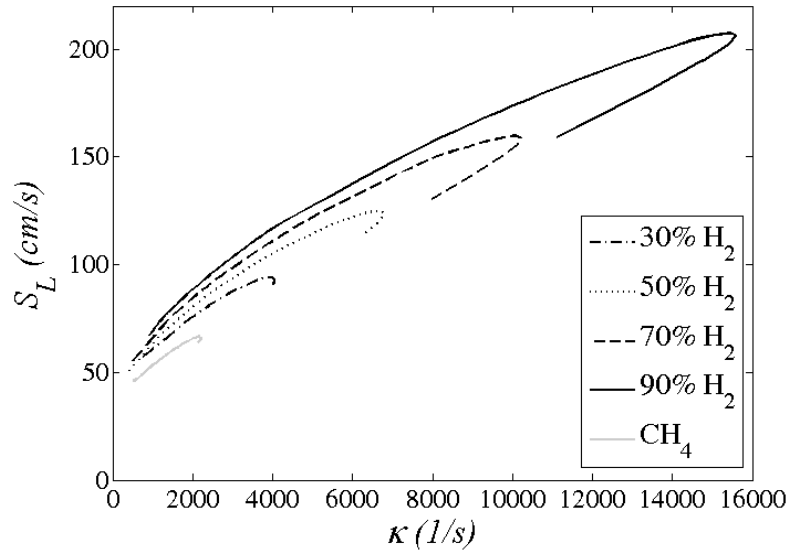
Figure 17: Stretch sensitivity calculations of constant $S_{L,0}$ mixtures (see Table 1 for stoichiometry values of each mixture).

4.1.   H₂/CO Sweeps at Constant $S_{L,0}$

This section presents data at various H₂/CO ratios at nominally constant $S_{L,0}$ for 12mm and 20mm burner diameters for inlet reactant mixture temperatures of 300K and 600K. Figure 18 and Figure 19 show plots of $S_{T,GC}/S_{L,0}$ for H₂/CO mixtures of 30/70, 50/50, 70/30, and 90/10 and mean flow velocities of 4, 10, 30, and 50 m/s for a 20mm burner diameter and preheat temperature of 600K. These two graphs plot the same data on a linear (Figure 18) and log (Figure 19) scale. For a given fuel composition, $S_{T,GC}$ increases monotonically with turbulence intensity. Also note the dependence of $S_{T,GC}$ on mean flow velocity. Each velocity result appears to lie on its own curve which is parallel to the lower velocity case, but does not intersect it at the same turbulence intensity. See Driscoll [10] for a discussion of mean velocity effects.

The main observation from this data is the monotonically increasing value of $S_{T,GC}$ with H₂ levels. Moreover, the data indicate that these fuel effects persist even at very high turbulence intensities.

Also included on these graphs are several measured or predicted S_T correlations. Some caution should be exercised in comparing these with the data, because of the definition dependence of S_T noted earlier. Bradley's equation [45] is given by:

$$\frac{S_T}{SS_{LL}} = 1.52 \frac{u'}{}$$ (7)

This is a theoretical result derived from considerations of the fractal characteristics of high intensity turbulent flames. It was derived using theoretically and experimentally obtained values for the fractal dimension and turbulent dissipation coefficients. As a result, the analysis appears to lend itself to a local definition of turbulent flame speed such as $S_{T,LC}$ or $S_{T,LD}$. A similar expression, derived from a different theoretical approach, was proposed by Anand and Pope [46], with a constant of 1.5.

Schelkin's expression [47] is given by:

$$\frac{S_T}{S_L} = \left[1 + \left(2\frac{u'}{S_L}\right)^2\right]^{0.5} \tag{8}$$

This is also a theoretical result that most closely corresponds to $S_{T,LC}$ or $S_{T,LD}$ using Damkohler's approach to wrinkled flames where the turbulent structures are much larger than the laminar flame thickness [45].

Yakhot [48] also developed the following theoretical expression, valid again for high turbulence intensity flames using renormalization approaches. Again, this expression most closely corresponds to $S_{T,LC}$ or $S_{T,LD}$.

$$\frac{S_T}{S_L} = \exp\left[\left(\frac{S_T}{S_L}\right)^2 \bigg/ \left(\frac{u'}{S_L}\right)^2\right] \tag{9}$$

Kobayashi *et al.* [49] developed a correlation from experimental data for CH_4/air and C_2H_4/air turbulent Bunsen flames that included pressure effects.

$$\frac{S_T}{S_L} = 2.9\left[\left(\frac{P u'}{P_0 S_L}\right)\right]^{0.38} \tag{10}$$

This value of S_T was based upon the $<c> = 0.5$ contour and corresponds to the global consumption speed definition. Figure 18 and Figure 19 show that the correlation over-predicts $S_{T,GC}$ for our CH_4/air data, but generally follows the observed trend. One possibility for this is that the turbulence intensity quoted by Kobayashi *et al.* [34] is only the axial RMS, while

turbulence intensity used in the current study is the total RMS which includes axial as well as radial and azimuthal components. Under the assumption that the turbulence intensity quoted by Kobayashi only included axial RMS fluctuations and assuming they had isotropic turbulence, their correlation was adjusted to include all three components of the RMS fluctuations. This new curve fit is labeled "Kobayashi (isotropic)" in Figure 18 and Figure 19. In order to examine this effect further, the relationship between our measured axial RMS and total RMS was found to be $u'' = u'_{rms}/\sqrt{3}$. This relationship was then used to again adjust the turbulence intensity values reported by Kobayashi. This curve is labeled "Kobayashi (adjusted)". As shown in Figure 18 and Figure 19, both of the adjusted correlations under-predict the values found, however, the original correlation of Kobayashi and the one adjusted for isotropic turbulence bracket the CH_4 values obtained in this experiment.

Figure 18: Variations of turbulent flame speed, $S_{T,GC}$, with turbulence intensity, u'_{rms}, normalized by $S_{L,0}$ at various mean flow velocities and H_2/CO ratios (linear plot).

Figure 19: Variations of turbulent flame speed, $S_{T,GC}$, with turbulence intensity, u'_{rms}, normalized by $S_{L,0}$ at various mean flow velocities and H_2/CO ratios (log-log plot).

The effects of H_2 level upon $S_{T,GC}/S_{L,0}$ at a fixed turbulence intensity is plotted in Figure 20. This graph shows an essentially linear dependence of $S_{T,GC}/S_{L,0}$ upon H_2 levels in the fuel over the investigated range. The point at 0% H_2 corresponds to the CH_4 flame. Note that the difference in flame speeds between low and high H_2 flames for the H_2/CO blends and the CH_4/air and H_2/CO/air flames is significant, being as large as two and three, respectively.
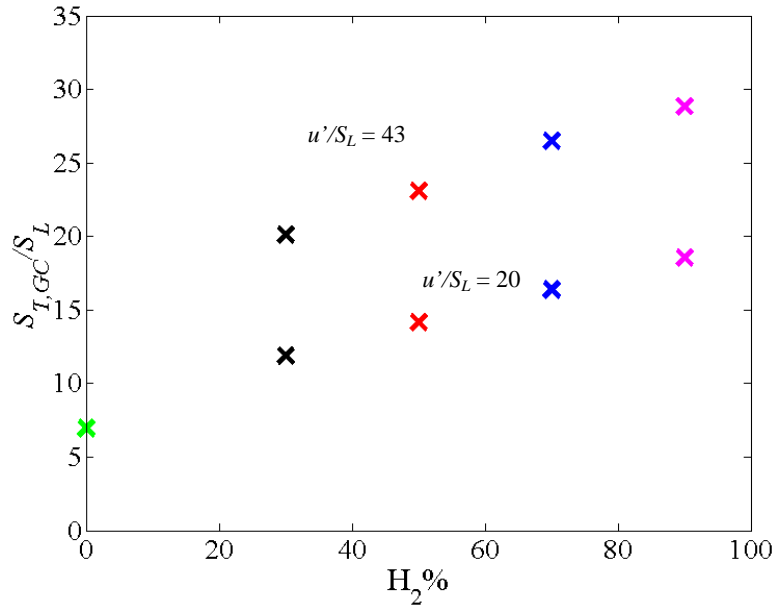
Figure 20: $S_{T,GC}/S_{L,0}$ variation with H_2 content for $u'_{rms}/S_{L,0}$ = 20 and 43 at $S_{L,0}$ = 34 cm/s.

The data for the 12 mm burner at various H_2/CO ratios at nominally constant $S_{L,0}$ for an inlet reactant mixture temperature of 300K are summarized in Figure 21 and Figure 22, which plot $S_{T,GC}/S_{L,0}$ for H_2/CO blends at mean flow velocities of 20, 30, and 50 m/s. These two graphs plot the same data on a linear (Figure 21) and log (Figure 22) scale.

Figure 21: Variations of turbulent flame speed, $S_{T,GC}$, with turbulence intensity, u'_{rms}, normalized by $S_{L,0}$ at various mean flow velocities and H_2/CO ratios for the 12 mm burner (linear plot).

Figure 22: Variations of turbulent flame speed, $S_{T,GC}$, with turbulence intensity, u'_{rms}, normalized by $S_{L,0}$ at various mean flow velocities and H_2/CO ratios for the 12 mm burner (log plot).

From Figure 17 and Figure 20 the length scale sensitivity of the turbulent flame speed is clearly seen. At a given fuel composition, turbulence intensity, and mean flow velocity the larger burner diameter has a higher turbulent consumption speed. These differences are about 50% for 50 m/s and 60% for 30 m/s.

Although not the primary focus of this study, the mean flow dependencies at a given fuel composition are worthy of mention. First, these data clearly show the well known dependence of $S_{T,GC}$ upon U_0, a fact highlighted in [10, 50]. Each velocity result appears to lie on its own curve, which is parallel to the lower velocity case, but does not intersect it at the same turbulence intensity. This is particularly evident for $u'_{rms}/S_{L,0} = 10$ at $U_0 = 10$ and 30 m/s, and $u'_{rms}/S_{L,0} = 5$ for $U_0 = 4$ and 10 m/s where $S_{T,GC}/S_{L,0}$ differs by 100% and 36% for the 90% H_2 mixture, respectively. This mean flow dependence is less obvious at the $u'_{rms}/S_{L,0} = 23$ case between the $U_0 = 30$ and 50 m/s cases, presumably because the fractional variation in U_0 is much smaller in this case.

In addition to the atmospheric, non-preheated data presented thus far, turbulent flame speed data has also been taken at preheat conditions with an inlet mixture temperature of $T_u = 600K$. The data, presented in Figure 23, are for mean flow velocities of 30 and 50 m/s and a fixed laminar flame speed of $S_{L,0} = 200$ cm/s. The laminar flame speed was increased in order to keep the equivalence ratio from becoming very lean. As before, the turbulent flame speed is a function of fuel composition, with increasing $S_{T,GC}$ as H_2 percentage increases. The data tend to be in the lower turbulence intensity regime, which is mainly due to the increased $S_{L,0}$ and lower mass flow rates for a given mean flow velocity.
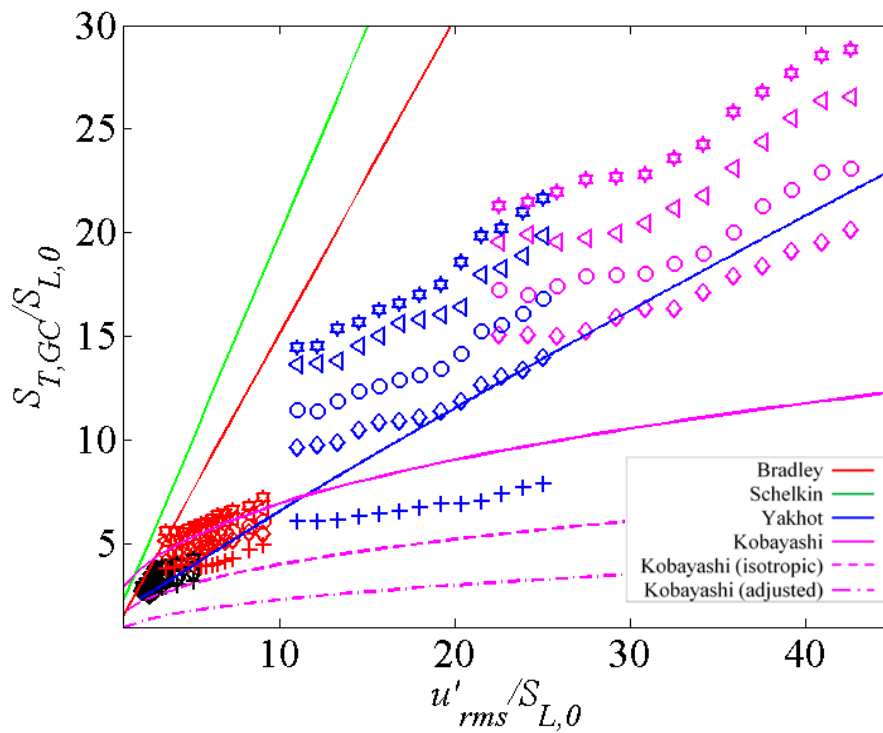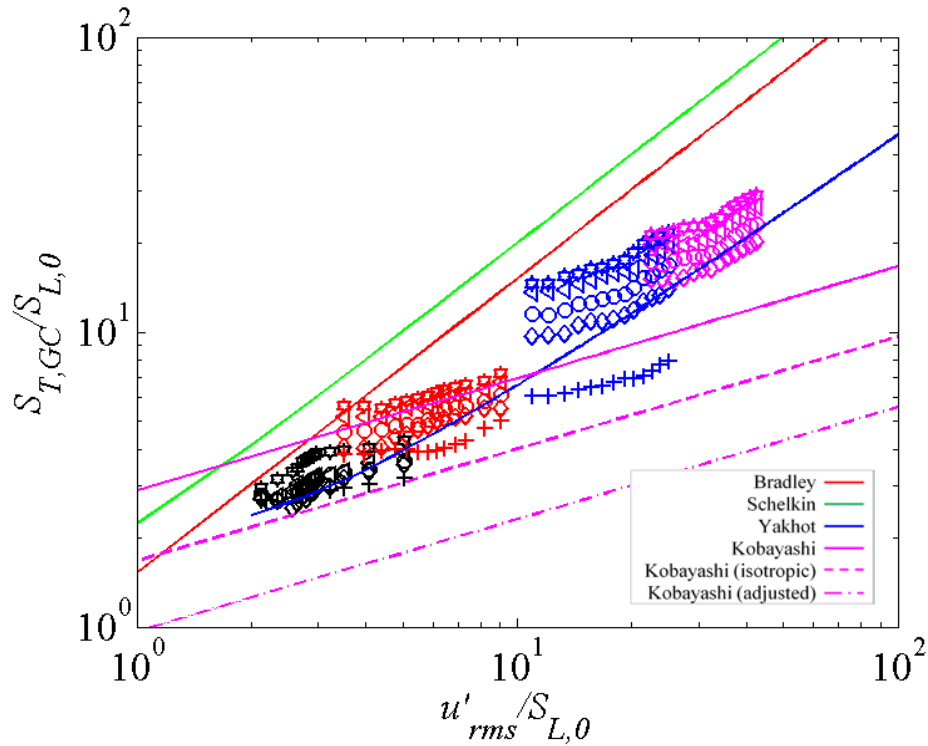
Figure 23: Variations of turbulent flame speed, $S_{T,GC}$, with turbulence intensity, u'_{rms} normalized by $S_{L,0}$ at various mean flow velocities and H_2/CO ratios for a preheat temperature of 600 K.

4.2.   Equivalence Ratio Sweeps

In order to determine the effect of varying $S_{L,0}$ at fixed H_2 fractions, equivalence ratio sweeps were also performed at fixed H_2 contents of 30 and 60% for three equivalence ratios using the 20 mm burner diameter. The symbols used for Figure 24 through Figure 27 are presented in Table 4. Figure 24 and Figure 25 show the results for a 60% H_2 mixture at $\phi = 0.4$, 0.6, 0.8 for mean flow velocities of 4, 10, 30, and 50 m/s. Note that $S_{L,0}$ is not held nominally constant for these data, as it was in the prior section.
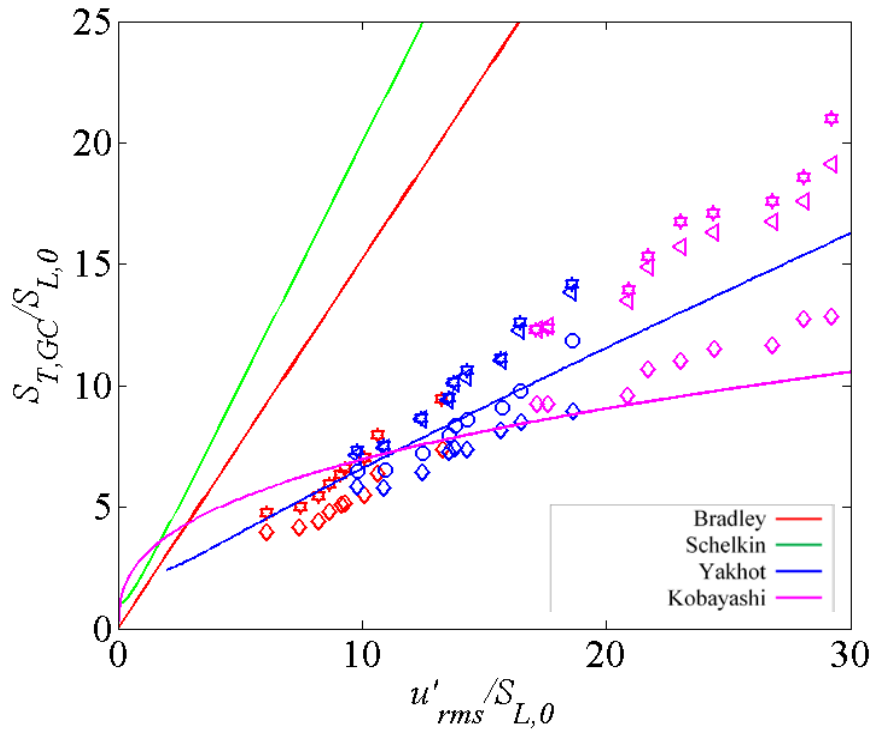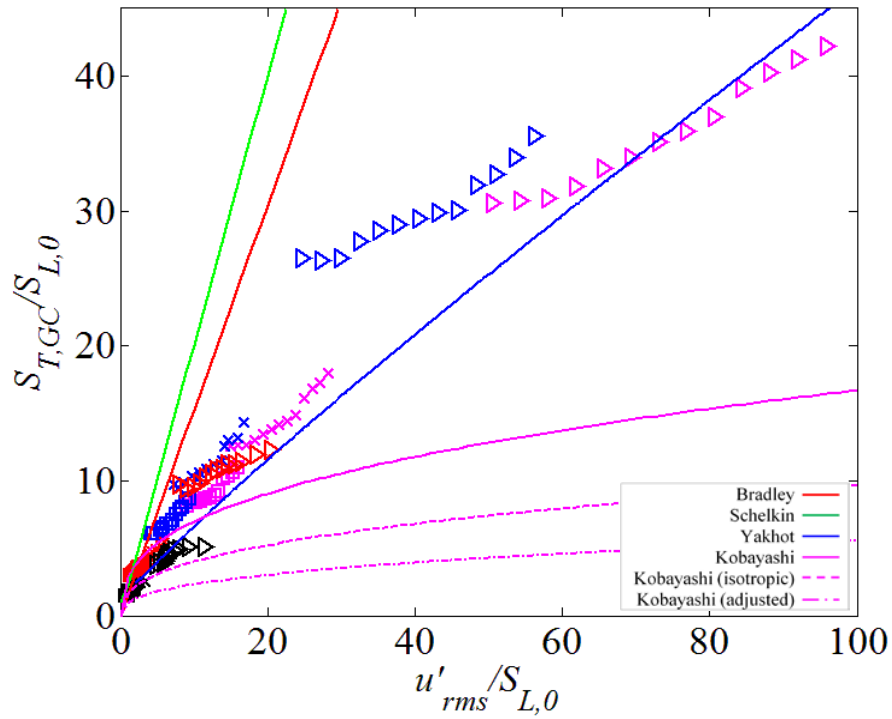
Figure 24: Variations of turbulent flame speed, $S_{T,GC}$, with turbulence intensity, u'_{rms}, normalized by $S_{L,0}$ at various mean flow velocities and equivalence ratios at a fixed H_2 content of 60% (linear plot).
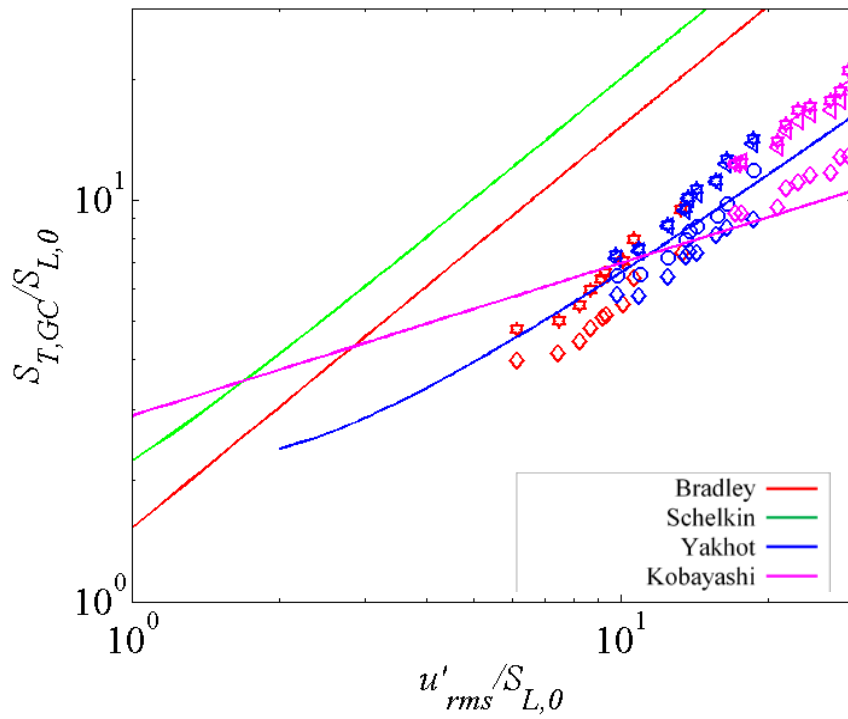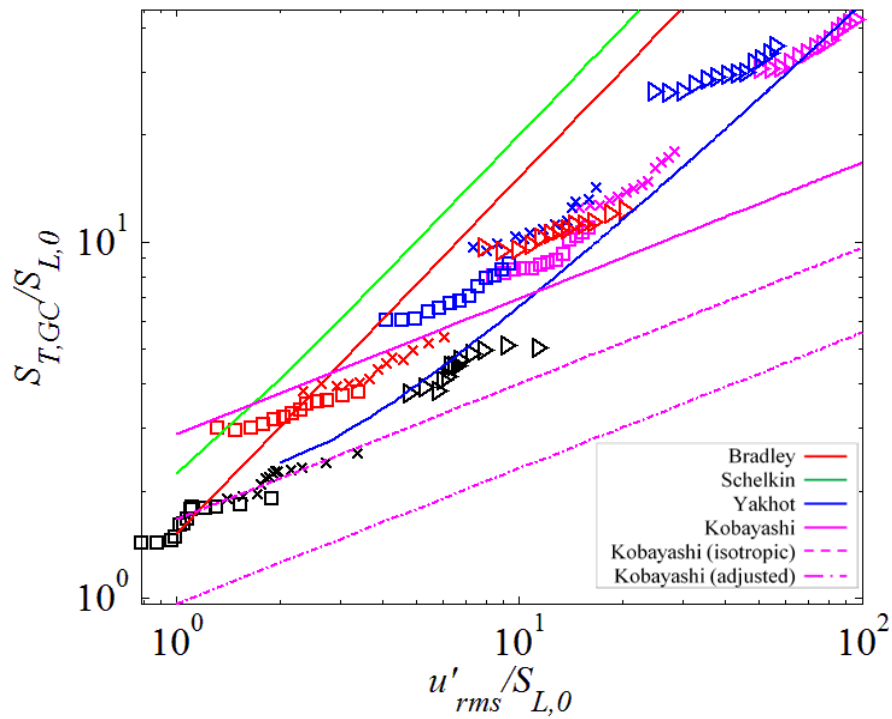

Figure 25: Variations of turbulent flame speed, $S_{T,GC}$, with turbulence intensity, u'_{rms}, normalized by $S_{L,0}$ for various mean flow velocities and equivalence ratios at a fixed H_2 content of 60% (log-log plot).

As in Figure 18 and Figure 19, the S_T correlations discussed above have also been plotted. From Figure 25, which is the log-log version of Figure 24, it is seen that the data generally fall within the band formed by the correlations given by Equation (7) and Equation (9). Furthermore, the slope of the data seems to agree quite well with Kobayashi's correlation, given by Equation (11), particularly at the low to intermediate $u'/S_{L,0}$ ranges.

Figure 26 shows the results for a 30% H_2 mixture at $\phi = 0.59, 0.7, 0.8$ for mean flow velocities of 4, 10, 30, and 50 m/s, for the 20mm burner diameter and inlet reactant mixture temperature of 300K.
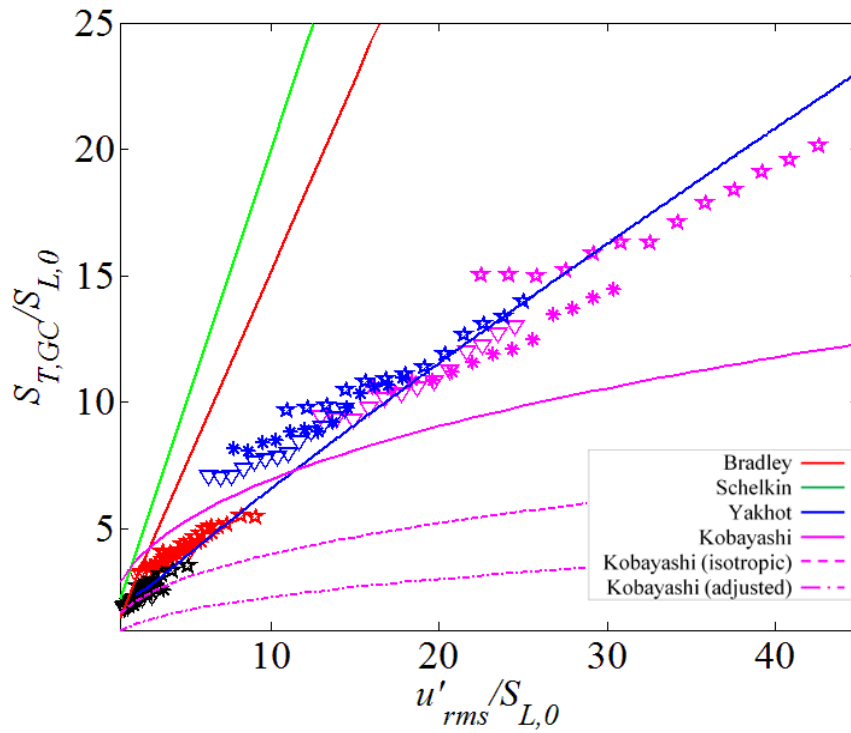
Figure 26: Variations of turbulent flame speed, $S_{T,GC}$, with turbulence intensity, u'_{rms}, normalized by $S_{L,0}$ at various mean flow velocities and equivalence ratios at a fixed H_2 content of 30% (linear plot).
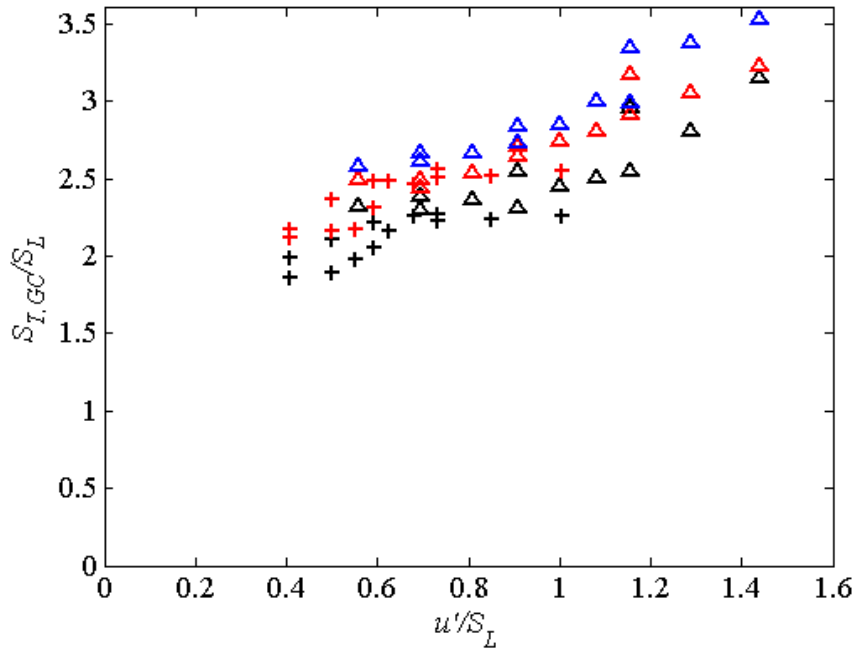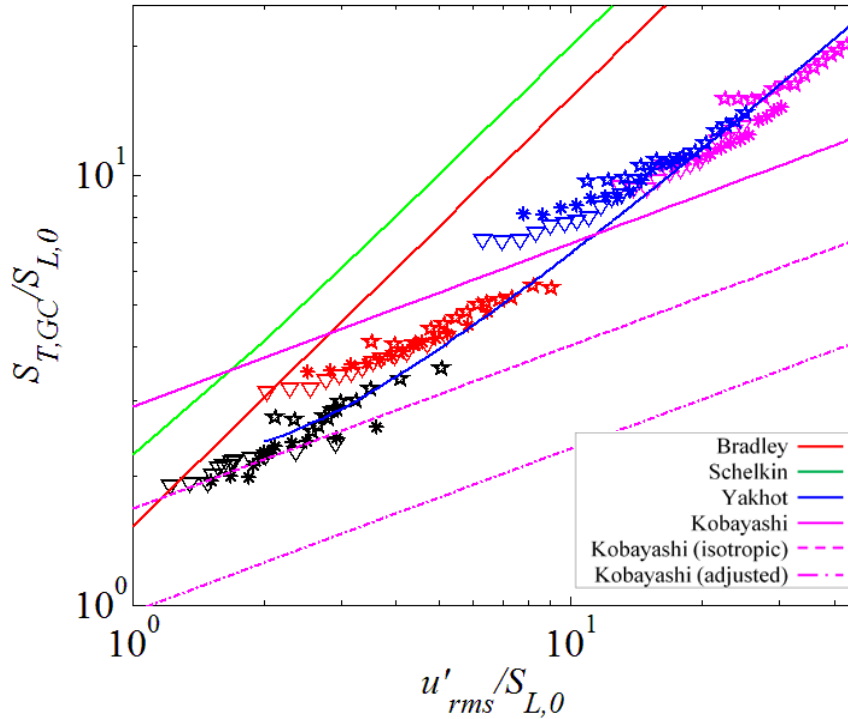
Figure 27: Variations of turbulent flame speed, $S_{T,GC}$, with turbulence intensity, u'_{rms}, normalized by $S_{L,0}$ at various mean flow velocities and equivalence ratios at a fixed H_2 content of 30% (log-log plot).

Again from Figure 27, it can be seen the data generally fall within the band created by the stretch-free correlations. Furthermore, since the $u'_{rms}/S_{L,0}$ range investigated with the 30/70 H_2/CO mixture is smaller, it is easier to see that the correlation given by Equation (9) is a close match.

5.   Analysis of Flame Speed Data

These data are consistent with prior studies showing that stretch sensitivity of the reactants has an important impact on the turbulent flame speed [9-10]. This point is shown in Figure 28, which plots the dependence of $S_{T,GC}/S_{L,0}$ of the data reported in this paper upon calculated Markstein length of the reactants, l_M (see Figure 28), at two different turbulence intensities for the constant $S_{L,0}$ studies. The point located at $l_M = -0.02$ for $u'_{rms}/S_{L,0} = 20$ corresponds to the methane-air mixture at $\Phi = 0.9$. Note the monotonically increasing value of $S_{T,GC}$ with $|l_M|$. Also the difference in flame speeds between low and high H_2 flames for the H_2/CO blends and the CH_4/air and H_2/CO/air flames is significant, being as large as two and three, respectively.
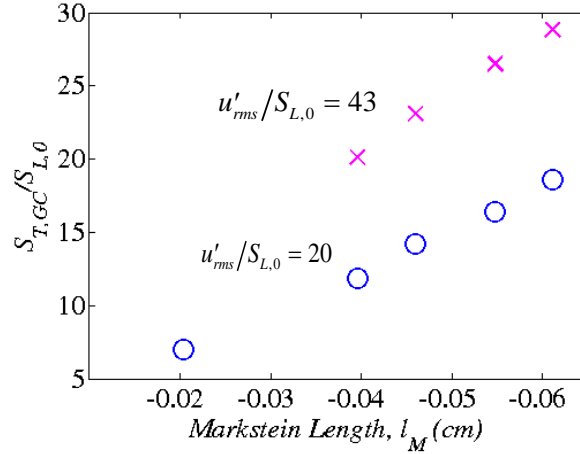
Figure 28: Dependence of $S_{T,GC}/S_{L,0}$ upon Markstein length, l_M, for $u'_{rms}/S_{L,0} = 20$ and 43 at $S_{L,0} = 0.34$ m/s.

A common approach for scaling turbulent flame speeds is to use the consumption based definition [10]:

$$S_T = \frac{\langle S_L A \rangle}{A_0} \tag{11}$$

Or, by introducing the stretch factor, I_0 [51-52]:

$$S_T = \frac{S_{L,0} \langle I_0 A \rangle}{A_0} \tag{12}$$

For stretch insensitive flames, the I_0 factor equals unity, leading to the classical S_T scaling described by Damköhler [53]. For stretch sensitive flames, one is left with the function $\langle I_0 A \rangle$, which requires understanding the correlation between local flame speed and flame area. Assuming that these functions are uncorrelated, i.e., that $\langle I_0 A \rangle = \langle I_0 \rangle \langle A \rangle$ leads to the erroneous prediction that the mixture's stretch sensitivity should not influence S_T [54]. This prediction follows from measurements and computations which show that the flame curvature PDF is roughly symmetric about $\kappa = 0$ [55-58], implying that regions of enhanced and diminished local consumption rate should roughly cancel and, thus, that $\langle I_0 \rangle \approx 1$. Hydrodynamic strain, which is not symmetric about $\kappa = 0$ [57-59] does introduce a non-unity $\langle I_0 \rangle$ value, but it seems unlikely that this effect is significant enough to explain the appreciable fuel effects reported here and in the literature.

However, it can easily be seen that assuming uncorrelated A and I_0 passes over key physics: in particular, there are implicit I_0 effects in the $<A>$ term because the local flame speed and area are highly correlated. For example, if the positively curved leading point of the flame has a higher local flame speed, it will propagate at a faster speed into the unburned reactants, increasing flame area accordingly. In the same way, the slower, negatively curved trailing point of the flame will lag backwards, also increasing flame area.

Given the implicit presence of the I_0 term in the $<A>$ term, modeling approaches based upon leading points concepts [9, 22-23] may be more useful for explicitly bringing out stretch sensitivity effects. The leading points are roughly defined as the necessarily positively curved points on the turbulent flame front that propagate farthest into the reactants. It has been argued that the propagation speed of these points with respect to the average flow velocity control the overall turbulent flame speed [23]. As a result, fuel/air mixtures with negative Markstein numbers will have enhanced laminar flame speeds at the positively curved leading points, resulting in larger displacement speeds. This basic leading points argument can be readily understood from the simple model problem of a flat flame propagating into a spatially varying velocity field with zero mean flow velocity, as depicted in Figure 29.
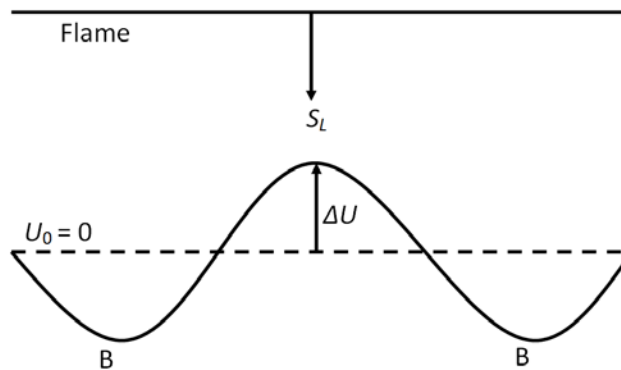
Figure 29: Model problem of a flat flame propagating into a spatially varying flow field.

If we assume that S_L remains constant, then it is seen that the portion of the flame at the lowest velocity point propagates out the fastest. In the lab-fixed coordinate system, the flame at Point B moves at a speed of $S_L + (\Delta u)_{LP}$, where the subscript "LP" denotes the leading point. Moreover, it can easily be shown by a front tracking computation that, after an initial transient, the entire front reaches a stationary shape and propagation speed which has the same value; i.e., $S_D = S_L + (\Delta u)_{LP}$. As such, the overall displacement speed is controlled by the leading points of

the flame that propagate into the lowest velocity regions ahead of the flame. Note also that the flame area would increase as well, but this is an *effect* of the higher displacement speed, not the *cause*.

In reality, the positively curved leading point of the flame will have an altered flame speed, $(S_L)_{LP} = S_{L,0} + (S_L')_{LP}$, where $(S_L')_{LP}$ is the modification of the un-stretched laminar flame speed at the leading point, because of the mixtures nonzero Markstein length. If the mixture has a negative Markstein number, then the flame speed at this point will further increase, causing an increase in curvature, further increasing the local flame speed. This is, in essence, a restatement of the fact that such negative Markstein length mixtures are thermo-diffusively unstable [11]. As a result, the above expression can be modified to take into account the flame speed augmentation:

$$S_{DLL}S_{L}S_{L}u+ + \Delta_{,0} \quad (\quad ')_{LPLP} (\quad) \tag{13}$$

The key difference to note from this scaling approach relative to Eq. (8) is that this focuses on a local flame characteristic – namely the positively curved leading point – as opposed to some global average, $<I_0A>$, which obscures the stretch effect.

The key problem lies in scaling $(S_L')_{LP}$. If the positively curved leading point is weakly stretched, then $(S_L')_{LP} \sim l_M\kappa_{LP}$. This switches the problem to scaling the strain statistics conditioned on the leading point of the flame, κ_{LP}, an important fundamental problem in turbulent combustion; see Lipatnikov and Chomiak [9] for discussion. Since the investigated mixtures are thermo-diffusively unstable, the $\kappa=0$, $S_L = S_{L,0}$ points are 'repelling' points in flame strain rate space. In other words, any perturbation of a flat flame will grow, causing an increase in curvature of the positively curved leading edge of the flame. This increase in curvature causes a further increase in flame speed and, therefore, a further increase in curvature, see Figure 30. In fact, as will be shown more rigorously in the subsequent discussion, $S_L = S_{L,max}$ is a steady-state 'attracting' point for a positively curved wrinkle. Moreover, the flame speed at the leading point, $(S_L)_{LP}$ is bounded by $S_{L,max}$ value; i.e., $S_{L,max} > (S_L)_{LP} > S_{L,0}$. For an opposed flow flame, $S_{L,max}$ can be directly extracted from the simulations shown in Figure 17. For example, this leads to the following inequality for the 30% H_2 blend: 95 cm/s $> (S_L)_{LP} > 34$ cm/s.
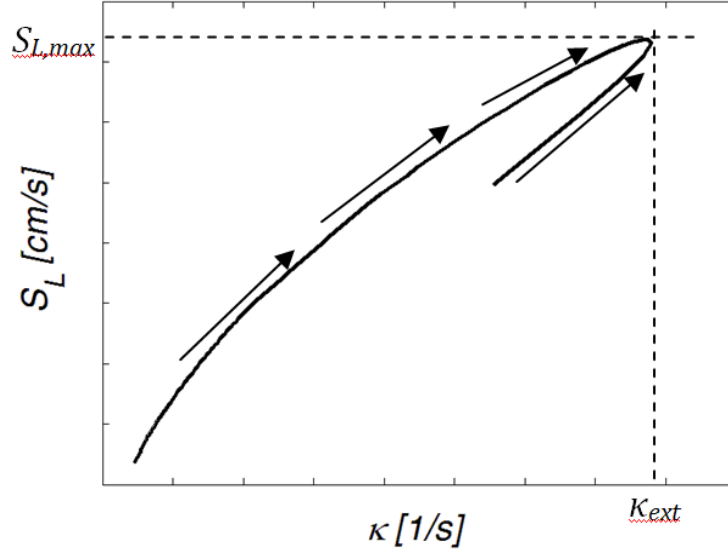
Figure 30: Example plot showing the 'attracting' nature of $S_{L,max}$

Substituting this $S_{L,max}$ value in for $(S_L)_{LP}$ and writing $(\Delta u)_{LP}$ as u'_{LP}, leads to the following:

$$\frac{S_{u_{LP}}}{SS_{Llmax,max}} \leq 1 \qquad ' \underline{\qquad} \qquad (14)$$

Note that this is nearly identical to Damköhler's classical result [53] where S_L has been replaced by $S_{L,max}$ and u' by u'_{LP}. Also note that by using u'_{LP}, the mean flow dependence discussed earlier is implicitly included in the model since the evolution of the turbulence between the burner exit and the flame front will be determined by a convective time scale that is controlled by the mean flow velocity [10].

On the basis of the scaling derived above, all the $S_{T,GC}$ data presented above are replotted using the $S_{L,max}$ normalization. Because of the mean flow dependencies noted earlier, we plot this data first at fixed flow velocities.
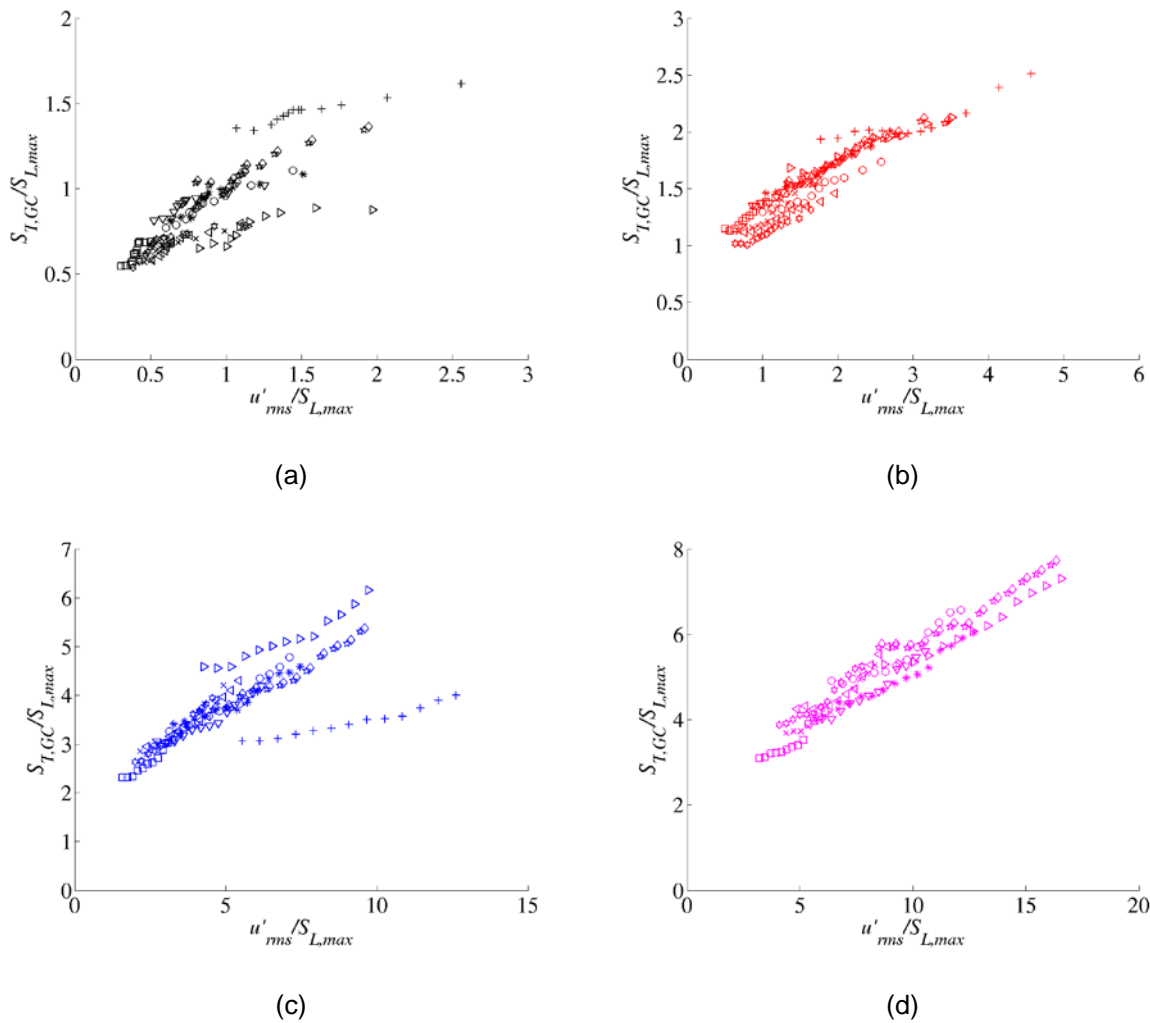
Figure 31: Variations of the turbulent flame speed, $S_{T,GC}$, with turbulence intensity u'_{rms} normalized by $S_{L,max}$ of both constant $S_{L,0}$ and equivalence ratio sweep studies for 20 mm burner grouped by mean flow velocities (a) 4 m/s (b) 10 m/s (c) 30 m/s (d) 50 m/s. (See Table 1 and Table 4 for legend)

Figure 26 shows that the data collapses generally well across all the mean flow velocities. There is some scatter that in the 4 m/s data that largely disappears at the higher flow velocities. Also, note that the 30 m/s CH_4/air data does not collapse with the H_2/CO data set while it collapses at 10 m/s and 4 m/s.

Figure 32 plots the entire 20 mm burner data set, which contains both the constant $S_{L,0}$ studies and the equivalence ratio sweep studies, while Figure 33 displays the renormalized 12 mm burner data.
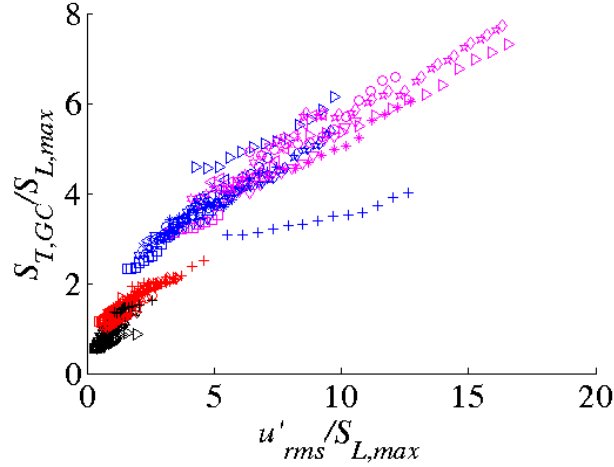
Figure 32: $S_{L,max}$ normalized $S_{T,GC}$ data for the 20 mm burner including constant $S_{L,0}$ and equivalence ratio sweep studies (see Table 1 and Table 4 for legend)
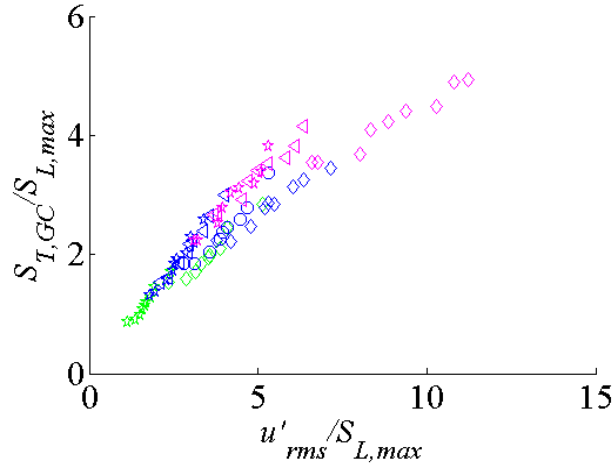
Figure 33: $S_{L,max}$ normalized $S_{T,GC}$ data for the 12 mm burner for constant $S_{L,0}$ studies (see Table 2 for legend)

From Figure 32 and Figure 33 it is clear that both data sets collapse very well, with the exception of the 30 m/s CH_4 data. In fact for the 20 mm constant $S_{L,0}$ data set, the variation in the normalized turbulent flame speed values for the 30/70 to 90/10 reduced from 50% to about 10% (for the 50 m/s case) between Figure 18 and Figure 32. Larger disparities (about 50% at $u'_{rms}/S_{L,max}$ = 12.5) are seen between the H_2/CO data and CH_4 data. This scatter and some caveats are discussed further in the following paragraphs.

First, some scatter is inevitable as the κ_{ext} and $S_{L,max}$ value are not constants for a given mixture but depends upon the strain profile the flame is subjected to [60] and the relative amount of curvature versus hydrodynamic induced flame stretch. For example, repeating these

calculations using nozzle separation distances ranging from 10 to 40 mm causes variations in $S_{L,max}$ of 5% for the 30/70 H_2/CO mixture. Moreover, this $S_{L,max}$ value is a function of the experimental configuration – in the opposed flow configuration, it is closely related to reaction zone impingement on the stagnation plane so that complete reaction is not possible [11]. Presumably, the $S_{L,max}$ at the leading point of the turbulent flame brush would be related to the strain rate associated with the highly curved leading edge, whose radius of curvature is bounded by the flame thickness.

Second, the local burning velocity at the leading point, $(S_L)_{LP}$ is not identically equal to $S_{L,max}$; rather, $S_{L,max}$ is simply an upper bound of an inequality. The reason that the $S_{L,max}$ correlation appears to work quite well because it can be shown that it is an attracting point and, in the "quasi-steady" limit where the turbulence evolves very slowly relative to the time scale over which the flame can adjust its position, that $(S_L)_{LP}$ will tend toward $S_{L,max}$. This point was made heuristically above, but it can also be shown formally by considering the following level set equation describing the flame's spatio-temporal dynamics,

$$\frac{\partial G}{\partial t} + \overrightarrow{\vec{v}G} \cdot \overrightarrow{S_L G} \quad {}_{L} \Big| \quad \Big| \tag{15}$$

This is a suitable model for the flame's dynamics, as Figure 17 shows that the data falls primarily in the corrugated flamelets and thin reaction zone regimes. This equation can be treated analytically in the low turbulence intensity limit, where the flame position is a single-valued function of some coordinate $G = y - \xi(x, t)$, as shown in Figure 34 below.
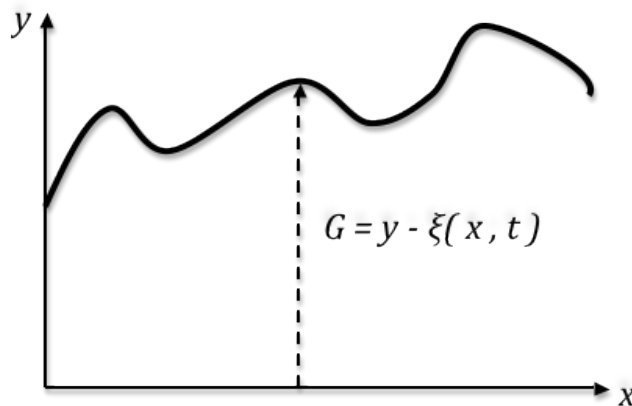

Figure 34: Coordinate system defining the instantaneous flame location, $\xi(x, t)$.

Writing the stretch sensitive flame speed as $S_L = S_{L,0}[1 + f(\kappa)]$, we obtain:

$$-\frac{\partial \xi}{\partial t} - U\frac{\partial \xi}{\partial x} + V = S_{L,0}\left[1 + f(\kappa)\right]\left[1 + \left(\frac{\partial \xi}{\partial x}\right)^2\right]^{1/2} \tag{16}$$

Differentiating this expression with respect to x, and substituting g for $\partial \xi/\partial x$:

$$-\frac{\partial g}{\partial t} - \frac{\partial}{\partial x}(Ug) + \frac{\partial V}{\partial x} = S_{L,0}\left(1 + g^2\right)^{1/2}\frac{\partial f}{\partial \kappa}\frac{\partial \kappa}{\partial x} + S_{L,0}\left[1 + f(\kappa)\right]\frac{g}{\left(1 + g^2\right)^{1/2}}\frac{\partial g}{\partial x} \tag{17}$$

A necessary condition for leading points, located at the points, x_{LP}, is that $g(x_{LP}, t) = 0$ and $\partial g(x_{LP}, t)/\partial x < 0$. We can determine the asymptotic tendencies of these leading points in a quiescent medium by taking the steady state limit of this equation by setting $\partial g/\partial t = 0$ and $U = V = 0$. Furthermore, by explicitly writing the curvature induced strain, κ, as $\frac{\partial g/\partial x}{\left(1 + g^2\right)^{3/2}}$, Equation (17) can then be expressed as:

$$0 = S_{L,0}\left(1 + g_{ss}^2\right)^{1/2}\frac{\partial f}{\partial \kappa}\left[\frac{\partial^2 g_{ss}}{\partial x^2}\left(1 + g_{ss}^2\right)^{-3/2} - 3g_{ss}\left(1 + g_{ss}^2\right)^{-5/2}\left(\frac{\partial g_{ss}}{\partial x}\right)^2\right]$$
$$+ S_{L,0}\left[1 + f(\kappa)\right]\frac{g_{ss}}{\left(1 + g_{ss}^2\right)^{1/2}}\frac{\partial g_{ss}}{\partial x} \tag{18}$$

Setting $g_{ss} = 0$ shows that the following necessary condition is satisfied at the leading point:

$$\frac{\partial f}{\partial \kappa}\frac{\partial^2 g_{ss}}{\partial x^2} = 0 \tag{19}$$

Equation (19) shows that the steady state leading points must occur where $\partial f/\partial \kappa = 0$, which coincides with the location of $S_L = S_{L,max}$. Physical arguments can also be used to show that this is a stable attracting point if $\partial^2 f/\partial \kappa^2 < 0$, and that $\partial g/\partial x < 0$ at this $\partial f/\partial \kappa = 0$ point.

The above analysis clearly shows that equating $(S_L)_{LP}$ with $S_{L,max}$ is appropriate in the "quasi-steady" limit of slow turbulent fluctuations. In reality, the leading points continuously evolve in time, as the character of the turbulent fluctuations change, causing points to move back

and forth, with the leading points at a given instant approximately corresponding to the points of local minimum in velocity. Further analysis is needed to understand these unsteady effects.

From the derivation of the Equation (14), it is evident that this scaling may be more suitable for a local displacement turbulent flame speed definition.

Finally, note that the $S_{T,GC}$ data reported here by virtue of Equation (2) necessarily average over potentially significant variations in local flame speeds whereas the scaling shown in Equation (14) is essentially valid at a single point on the instantaneous flame front. As a result, adjustments to suitably average over a spatially developing flow field and flame brush are required. Nonetheless, the very good collapse of the large data set obtained here provides strong evidence for the basic validity of the scaling argument shown in Equation (14). Note that this argument will need revisiting for $l_M > 0$ flames, where the attracting point argument discussed above requires modification.

6. **Conclusions**

This report outlines the key data-sets and results obtained during the course of this three-year project involved with making turbulent flame speed measurements of H_2/CO fuel blends. Flame speed measurements were obtained for atmospheric H_2/CO blends for mean flow velocities and turbulence intensities of $4<U_0<50$ and $1<u'_{rms}/S_{L,0}<100$ respectively for H_2 fuel contents of 30% to 90% by volume. Furthermore, the influence of turbulent length scales were investigated by making measurements using 12mm and 20mm burner diameters, and the influence of reactant temperatures were also investigated by taking measurements at 300K and 600K preheat temperatures.

These data clearly corroborate results from other studies that show significant sensitivity of $S_{T,GC}$ to fuel composition. For example, $S_{T,GC}$ in the 90% H_2 case is 3 times larger than the $\phi = 0.9$ CH_4/air mixture with the same $S_{L,0}$ value. An important conclusion from this work is that fuel effects on $S_{T,GC}$ highlighted above are not simply a low turbulence intensity phenomenon – they clearly persist over the entire range of turbulence intensities used in the measurements.

It is believed that observed fuel effects are due to the reactant mixture stretch sensitivity, which has a strong effect on the positively strained leading points of the turbulent flame brush for non-zero Markstein length fuels. These leading points propagate at a rate equal to the turbulent displacement speed. We showed that leading point concepts lead to a scaling law that

collapses much of the data. Furthermore, modeling the instantaneous flame front using the G-equation, we were also able to show that the flame speed at the leading point always tends towards $S_{L,max}$ in a quasi-steady flow, validating the choice of $S_{L,max}$ as parameter to correlate the $S_{T,GC}$ data.

References

1. LIEUWEN, T., YANG, V., *SYNGAS COMBUSTION*. 2009: CRC PRESS.
2. KLIMSTRA, J., *INTERCHANGEABILITY OF GASEOUS FUELS ? THE IMPORTANCE OF THE WOBBE-INDEX*. SAE TRANSACTIONS, 1986. **95**(6): P. 962-972.
3. MOLIERE, M., *BENEFITING FROM THE WIDE FUEL CAPABILITY OF GAS TURBINES: A REVIEW OF APPLICATION OPPORTUNITIES*. ASME PAPER# GT-2002-30017, 2002.
4. LIEUWEN, T., MCDONELL, V., PETERSEN, E., SANTAVICCA, D., *FUEL FLEXIBILITY INFLUENCES ON PREMIXED COMBUSTOR BLOWOUT, FLASHBACK, AUTOIGNITION, AND STABILITY*. JOURNAL OF ENGINEERING FOR GAS TURBINES AND POWER, 2008. **130**: P. 011506.
5. LIEUWEN, T.C., YANG, V., *COMBUSTION INSTABILITIES IN GAS TURBINE ENGINES (OPERATIONAL EXPERIENCE, FUNDAMENTAL MECHANISMS AND MODELING)*. PROGRESS IN ASTRONAUTICS AND AERONAUTICS, 2005.
6. FIGURA, L., LEE, J.G., QUAY, B.D., SANTAVICCA, D., *THE EFFECTS OF FUEL COMPOSITION ON FLAME STRUCTURE AND COMBUSTION DYNAMICS IN A LEAN PREMIXED COMBUSTOR*, IN *ASME PAPER # GT2007-27298*. 2007.
7. VAGELOPOULOS, C.M., EGOLFOPOULOS, F. N., *LAMINAR FLAME SPEEDS AND EXTINCTION STRAIN RATES OF MIXTURES OF CARBON MONOXIDE WITH HYDROGEN, METHANE, AND AIR*. SYMPOSIUM (INTERNATIONAL) ON COMBUSTION, 1994. **25**(1): P. 1317-1323.
8. LIPATNIKOV, A.N., CHOMIAK, J., *TURBULENT FLAME SPEED AND THICKNESS: PHENOMENOLOGY, EVALUATION, AND APPLICATION IN MULTI-DIMENSIONAL SIMULATIONS*. PROGRESS IN ENERGY AND COMBUSTION SCIENCE, 2002. **28**(1): P. 1-74.
9. LIPATNIKOV, A.N. AND J. CHOMIAK, *MOLECULAR TRANSPORT EFFECTS ON TURBULENT FLAME PROPAGATION AND STRUCTURE*. PROGRESS IN ENERGY AND COMBUSTION SCIENCE, 2005. **31**(1): P. 1-73.
10. DRISCOLL, J.F., *TURBULENT PREMIXED COMBUSTION: FLAMELET STRUCTURE AND ITS EFFECT ON TURBULENT BURNING VELOCITIES*. PROGRESS IN ENERGY AND COMBUSTION SCIENCE, 2008. **34**(1): P. 91-134.
11. LAW, C.K., *COMBUSTION PHYSICS*. 2006, NEW YORK: CAMBRIDGE UNIVERSITY PRESS. 431.
12. KIDO, H., ET AL., *INFLUENCE OF LOCAL FLAME DISPLACEMENT VELOCITY ON TURBULENT BURNING VELOCITY*. PROCEEDINGS OF THE COMBUSTION INSTITUTE, 2002. **29**(2): P. 1855-1861.
13. DANIELE, S., P. JANSOHN, AND K. BOULOUCHOS, *FLAME FRONT CHARACTERISTIC AND TURBULENT FLAME SPEED OF LEAN PREMIXED SYNGAS COMBUSTION AT GAS TURBINE RELEVANT CONDITIONS*, IN *PROCEEDINGS OF ASME TURBO EXPO 2009*. 2009: GT2009-59477, ORLANDO, FLORIDA.

14.   KARPOV, V.P. AND E.S. SEVERIN, *Turbulent combustion of mixtures of hydrogen and carbon monoxide.* COMBUSTION, EXPLOSION, AND SHOCK WAVES, 1982. **18**(6): P. 643-644.

15.   WU, M.S., ET AL., *Turbulent Premixed Hydrogen/Air Flames at High Reynolds Numbers.* COMBUSTION SCIENCE AND TECHNOLOGY, 1990. **73**(1): P. 327-350.

16.   GÜLDER, Ö.L., ET AL., *Flame front surface characteristics in turbulent premixed propane/air combustion.* COMBUSTION AND FLAME, 2000. **120**(4): P. 407-416.

17.   KITAGAWA, T., ET AL., *Turbulent burning velocity of hydrogen-air premixed propagating flames at elevated pressures.* INTERNATIONAL JOURNAL OF HYDROGEN ENERGY, 2008. **33**(20): P. 5842-5849.

18.   KOBAYASHI, H., Y. KAWABATA, AND K. MARUTA, *Experimental study on general correlation of turbulent burning velocity at high pressure.* SYMPOSIUM (INTERNATIONAL) ON COMBUSTION, 1998. **27**(1): P. 941-948.

19.   NAKAHARA, M. AND H. KIDO, *Study on the Turbulent Burning Velocity of Hydrogen Mixtures Including Hydrocarbons.* AIAA JOURNAL, 2008. **46**(7): P. 1569-1575.

20.   KIDO, H., ET AL., *Turbulent Burning Velocities of Two-Component Fuel Mixtures of Methane, Propane and Hydrogen.* JSME INTERNATIONAL JOURNAL SERIES B FLUIDS AND THERMAL ENGINEERING, 2002. **45**(2): P. 355-362.

21.   BETEV, A., V. KARPOV, AND E. SEMENOV, *Nonsteady phenomena in propagation of highly curved flames.* CHEMICAL PHYSICS REPORTS C/C OF KHIMICHESKAIA FIZIKA 1997. **16**: P. 1861-1868.

22.   KUZNETSOV, V.R. AND V.A. SABEL'NIKOV, *Turbulent Combustion of a Homogenous Mixture*, IN *Turblence and Combustion*, V.R. KUZNETSOV, V.A. SABEL'NIKOV, AND P.A. LIBBY, EDITORS. 1986, HEMISPHERE PUBLISHING CORPORATION: MOSCOW. P. 362.

23.   KARPOV, V.P., A.N. LIPATNIKOV, AND V.L. ZIMONT, *Flame curvature as a determinant of preferential diffusion effects in premixed turbulent combustion*, IN *Advances in Combustion Science: In honor of Ya. B. Zel'dovich*, W.A. SIRIGNANO, A.G. MERZHANOV, AND L. DE LUCA, EDITORS. 1997, AIAA: RESTON, VA. P. 235-250.

24.   KOBAYASHI, H., TAMURA, T., MARUTA, K., NIIOKA, T., WILLIAMS, F. A. *Burning Velocity of Turbulent Premixed Flames in a High-Pressure Environment*. 1996: COMBUSTION INSTITUTE.

25.   CHENG, R., K., *Turbulent Combustion Properties of Premixed Syngases*, IN *Syngas Combustion*, T. LIEUWEN, YANG, V., EDITOR. TO APPEAR.

26.   GOULDIN, F. AND R.K. CHENG. *International Workshop on Premixed Turbulent Flames*. AVAILABLE FROM: HTTP://EETD.LBL.GOV/AET/COMBUSTION/WORKSHOP/WORKSHOP.HTML.

27.   VIDETO, B.D. AND D.A. SANTAVICCA, *A Turbulent Flow System for Studying Turbulent Combustion Processes.* COMBUSTION SCIENCE AND TECHNOLOGY, 1991. **76**(1-3): P. 159-164.

28.   BÉDAT, B. AND R.K. CHENG, *Experimental Study of Premixed Flames in Intense Isotropic Turbulence.* COMBUSTION AND FLAME, 1995. **100**(3): P. 485-494.

29.   KORTSCHIK, C., T. PLESSING, AND N. PETERS, *Laser Optical Investigation of Turbulent Transport of Temperature Ahead of the Preheat Zone in a Premixed Flame.* COMBUSTION AND FLAME, 2004. **136**(1-2): P. 43-50.

30.   CROW, S.C. AND F.H. CHAMPAGNE, *Orderly structure in jet turbulence.* JOURNAL OF FLUID MECHANICS, 1971. **48**: P. 547-591.

31.   MAYO JR, W.T. *A DISCUSSION OF LIMITATIONS AND EXTENTIONS OF POWER SPECTRUM ESTIMATION WITH BURST-COUNTER LDV SYSTEMS.* in *INTERNATIONAL WORKSHOP ON LASER VELOCIMETRY.* 1974. WEST LAFAYETTE, INDIANA, PURDUE UNIVERSITY.

32.   TUMMERS, M.J., PASSCHIER, D. M., *SPECTRAL ESTIMATION USING A VARIABLE WINDOW AND THE SLOTTING TECHNIQUE WITH LOCAL NORMALIZATION.* MEASUREMENT SCIENCE AND TECHNOLOGY, 1996. **7**: P. 1541-1546.

33.   SMALLWOOD, G.J., ET AL., *CHARACTERIZATION OF FLAME FRONT SURFACES IN TURBULENT PREMIXED METHANE/AIR COMBUSTION.* COMBUSTION AND FLAME, 1995. **101**(4): P. 461-470.

34.   KOBAYASHI, H., ET AL., *BURNING VELOCITY OF TURBULENT PREMIXED FLAMES IN A HIGH-PRESSURE ENVIRONMENT.* PROCEEDINGS OF THE COMBUSTION INSTITUTE, 1996. **26**: P. 389-396.

35.   GRIEBEL, P., P. SIEWERT, AND P. JANSOHN, *FLAME CHARACTERISTICS OF TURBULENT LEAN PREMIXED METHANE/AIR FLAMES AT HIGH PRESSURE: TURBULENT FLAME SPEED AND FLAME BRUSH THICKNESS.* PROCEEDINGS OF THE COMBUSTION INSTITUTE, 2007. **31**(2): P. 3083-3090.

36.   SEITZMAN, J.M., ET AL., *IMAGING AND CHARACTERIZATION OF OH STRUCTURES IN A TURBULENT NONPREMIXED FLAME.* SYMPOSIUM (INTERNATIONAL) ON COMBUSTION, 23RD, 1990: P. 637-644.

37.   HANSON, R.K., *COMBUSTION DIAGNOSTICS: PLANAR IMAGING TECHNIQUES.* SYMPOSIUM (INTERNATIONAL) ON COMBUSTION, 21ST, 1986: P. 1677-1691.

38.   DASCH, C., *ONE-DIMENSIONAL TOMOGRAPHY- A COMPARISON OF ABEL, ONION-PEELING, AND FILTERED BACKPROJECTION METHODS.* APPLIED OPTICS, 1992. **31**(8): P. 1146–1152.

39.   BALLAL, D. AND A. LEFEBVRE, *THE STRUCTURE AND PROPAGATION OF TURBULENT FLAMES.* PROCEEDINGS OF THE ROYAL SOCIETY OF LONDON. SERIES A, MATHEMATICAL AND PHYSICAL SCIENCES, 1975. **344**(1637): P. 217-234.

40.   SMALLWOOD, G.J., GÜLDER, Ö L., SNELLING, D. R., DESCHAMPS, B. M., GÖKALP, I., *CHARACTERIZATION OF FLAME FRONT SURFACES IN TURBULENT PREMIXED METHANE/AIR COMBUSTION.* COMBUSTION AND FLAME, 1995. **101**(4): P. 461-470.

41.   DAVIS, S.G., ET AL., *AN OPTIMIZED KINETIC MODEL OF H2/CO COMBUSTION.* PROCEEDINGS OF THE COMBUSTION INSTITUTE, 2005. **30**(1): P. 1283-1292.

42.   SMITH, G.P., ET AL. *GRI-MECH 3.0.* AVAILABLE FROM: HTTP://WWW.ME.BERKELEY.EDU/GRI_MECH/.

43.   WU, C.K. AND C.K. LAW, *ON THE DETERMINATION OF LAMINAR FLAME SPEEDS FROM STRETCHED FLAMES.* SYMPOSIUM (INTERNATIONAL) ON COMBUSTION, 1985. **20**(1): P. 1941-1949.

44.   KEE, R., ET AL. *A COMPUTATIONAL MODEL OF THE STRUCTURE AND EXTINCTION OF STRAINED, OPPOSED FLOW, PREMIXED METHANE-AIR FLAMES.* 1989: ELSEVIER.

45.   BRADLEY, D., *HOW FAST CAN WE BURN?* SYMPOSIUM (INTERNATIONAL) ON COMBUSTION, 1992. **24**(1): P. 247-262.

46.   ANAND, M.S., POPE, S. B., *CALCULATIONS OF PREMIXED TURBULENT FLAMES BY PDF METHODS.* COMBUSTION AND FLAME, 1987. **67**(2): P. 127-142.

47.   SCHELKIN, K.I., *ON COMBUSTION IN TURBULENT FLOW.* ZH. TEKH. FIZ, 1943. **13**: P. 520-530.

48.   YAKHOT, V., *PROPAGATION VELOCITY OF PREMIXED TURBULENT FLAMES.* COMBUSTION SCIENCE AND TECHNOLOGY, 1988. **60**(1): P. 191-214.

49.   KOBAYASHI, H., *EXPERIMENTAL STUDY OF HIGH-PRESSURE TURBULENT PREMIXED FLAMES.* EXPERIMENTAL THERMAL AND FLUID SCIENCE, 2002. **26**(2-4): P. 375-387.

50.   FILATYEV, S.A., ET AL., *MEASURED PROPERTIES OF TURBULENT PREMIXED FLAMES FOR MODEL ASSESSMENT, INCLUDING BURNING VELOCITIES, STRETCH RATES, AND SURFACE DENSITIES.* COMBUSTION AND FLAME, 2005. **141**: P. 1-21.

51.   POINSOT, T. AND D. VEYNANTE, *THEORETICAL AND NUMERICAL COMBUSTION.* 2005: RT EDWARDS, INC.

52.   BRAY, K.N.C. AND R.S. CANT, *SOME APPLICATIONS OF KOLMOGOROV'S TURBULENCE RESEARCH IN THE FIELD OF COMBUSTION.* PROCEEDINGS: MATHEMATICAL AND PHYSICAL SCIENCES, 1991: P. 217-240.

53.   DAMKÖHLER, G., *THE EFFECT OF TURBULENCE ON THE FLAME VELOCITY IN GAS MIXTURES.* ZEITSCHRIFT ELECTROCHEM, 1940. **46**: P. 601-626.

54.   EL TAHRY, S.H., C. RUTLAND, AND J. FERZIGER, *STRUCTURE AND PROPAGATION SPEEDS OF TURBULENT PREMIXED FLAMES--A NUMERICAL STUDY.* COMBUSTION AND FLAME, 1991. **83**(1-2): P. 155-173.

55.   YUEN, F.T.C. AND Ö.L. GÜLDER, *PREMIXED TURBULENT FLAME FRONT STRUCTURE INVESTIGATION BY RAYLEIGH SCATTERING IN THE THIN REACTION ZONE REGIME.* PROCEEDINGS OF THE COMBUSTION INSTITUTE, 2009. **32**(2): P. 1747-1754.

56.   GOIX, P.J. AND I.G. SHEPHERD, *LEWIS NUMBER EFFECTS ON TURBULENT PREMIXED FLAME STRUCTURE.* COMBUSTION SCIENCE AND TECHNOLOGY, 1993. **91**(4): P. 191 - 206.

57.   RUTLAND, C. AND A. TROUVÉ, *DIRECT SIMULATIONS OF PREMIXED TURBULENT FLAMES WITH NONUNITY LEWIS NUMBERS.* COMBUSTION AND FLAME, 1993. **94**(1): P. 41-57.

58.   HAWORTH, D. AND T. POINSOT, *NUMERICAL SIMULATIONS OF LEWIS NUMBER EFFECTS IN TURBULENT PREMIXED FLAMES.* JOURNAL OF FLUID MECHANICS, 1992. **244**: P. 405-436.

59.   BAUM, M., ET AL., *DIRECT NUMERICAL SIMULATION OF H2/O2/N2 FLAMES WITH COMPLEX CHEMISTRY IN TWO-DIMENSIONAL TURBULENT FLOWS.* JOURNAL OF FLUID MECHANICS, 1994. **281**: P. 1-32.

60.   EGOLFOPOULOS, F.N., *GEOMETRIC AND RADIATION EFFECTS ON STEADY AND UNSTEADY STRAINED LAMINAR FLAMES.* PROCEEDINGS OF THE COMBUSTION INSTITUTE, 1994. **25**(1): P. 1375-1381.